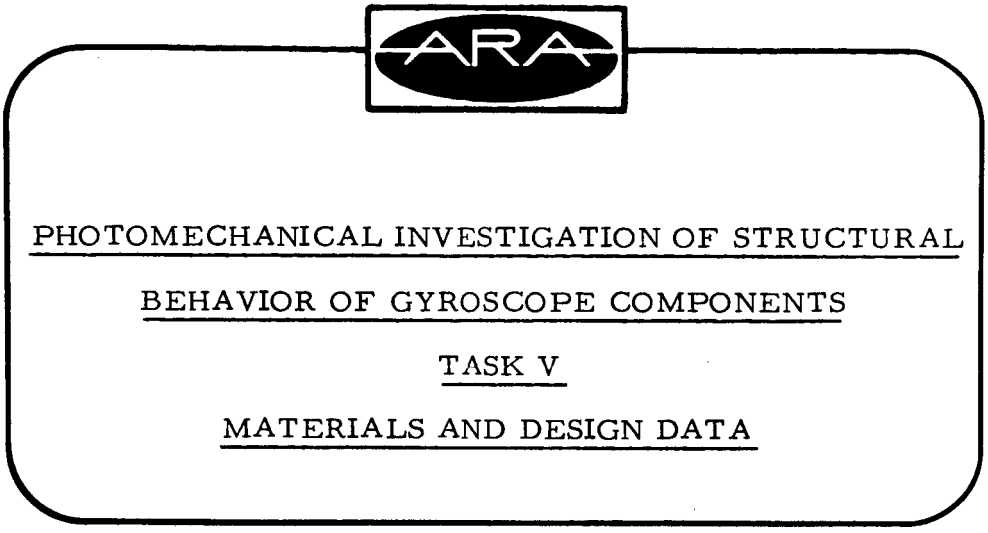

PHOTOMECHANICAL INVESTIGATION OF STRUCTURAL BEHAVIOR OF GYROSCOPE COMPONENTS

TASK V

MATERIALS AND DESIGN DATA

Final Technical Report No. ARA 284-21

September 1966

P. E. Kyle
R. Papirno
C. N. Tang
H. Becker

Prepared For

NAS8-11294

Astrionics Laboratory
National Aeronautics and Space Administration
Huntsville, Alabama

ALLIED RESEARCH ASSOCIATES, INC.
VIRGINIA ROAD • CONCORD, MASSACHUSETTS

PHOTOMECHANICAL INVESTIGATION OF STRUCTURAL BEHAVIOR OF GYROSCOPE COMPONENTS

TASK V

MATERIALS AND DESIGN DATA

Summary

This fifth report completes the 22 months of investigations by Allied Research into thermal, structural, materials, and design problems on advanced gyroscopes and accelerometers subjected to temperature, inertia, and impact. The latest data are preceded by a summary of the total project which recounts the results and highlights the major contributions.

Important results and conclusions from this latest phase are as follows:

1. Microplasticity data were obtained for S 100 and I 400 beryllium, for 52100 steel, for Lockalloy, and for Elkonite.
2. The initial microinch offset yield strength for S 100 was found to be approximately 2000 to 2500 psi whereas for I 400 values of about 7000 psi were found.
3. Hardly any significant variations in corrosion characteristics were observed in S 100, I 400, and Lockalloy.
4. Dislocation density measurements on S 100 indicated significant residual strain in the as-received condition in spite of the specification requirements of stress relieving.
5. Design charts were constructed for AB5-K8 rectangular fork proportions yielding equal rigidities in the two transverse directions and resisting a range of temperature differences and impact loads for a variety of fork/shaft material combinations.

The major accomplishments of the 22 months investigation were the identification of the superiority of I 400 beryllium alloy over S 100 alloy, efficient theoretical procedures for the determination of fork and shaft temperatures under steady state and transient conditions, and the construction of design charts for rapid identification of efficient fork geometries for a variety of fork/shaft material combinations.

TABLE OF CONTENTS

LIST OF FIGURES

LIST OF FIGURES (Continued)

LIST OF SYMBOLS

b	The width of fork, i. e., the dimension of fork in the direction normal to the shaft, in.
c	Clamp flexibility in terms of percent of $(\frac{\theta}{m})_f$.
E	Young's Modulus of elasticity, psi
E_f, E_s	Young's Modulus of elasticity for fork and shaft respectively, psi
f	Subscript for fork
F_x	Applied force in x direction, i. e., parallel to the shaft, lb.
F_y	Applied force in y direction, i. e., normal to the shaft, lb.
g	Acceleration of gravity
h	The depth of fork, i. e., the dimension of fork in the direction parallel to the shaft, in.
I	Moment of inertia, in^4
I_1	Moment of inertia of shaft corresponding to the smallest section, in^4
I_x	Moment of inertia of fork in x direction, in^4
I_y	Moment of inertia of fork in y direction, in^4
I_f	Moment of inertia of fork, in^4
I_s	Effective moment of inertia of shaft for computing $(\delta/S)_{sh}$, in^4
I_s^*	Effective moment of inertia of shaft for computing $(\theta/m)_s$, in^4
ℓ_f	The height of fork, in.
ℓ_s	The total length of shaft, in.
M	Moment at the ends of the shaft, in. lb.
M_o	Moment at the root of fork, in. lb.
P	Thrust in the shaft, lb.
S	Shear force normal to the shaft, lb.
W	Total weight of rotor, stator, and shaft, lb.

LIST OF SYMBOLS (Continued)

x	coordinate
y	coordinate
Δ_x, Δ_y	Deflections of upper end of fork in x and y direction, respectively in.
$\ddot{\Delta}_x, \ddot{\Delta}_y$	Accelerations of rotor in x and y directions respectively
$(\theta/p)_f$	Rotation of the upper end of fork caused by an unit shear
$(\theta/m)_f$	Rotation of the upper end of fork caused by an unit end moment
$(\theta/m)_c$	Rotation of the clamp caused by an unit moment
$(\theta/m)_s$	Rotation of the end of shaft caused by unit pure moment
$(\delta/p)_f$	Deflection of the upper end of fork caused by an unit end shear
$(\delta/m)_f$	Deflection of the upper end of fork caused by a unit shear at the center, the center being cut
α_s	Thermal coefficient of linear expansion, in/in/$^\circ$F
β_1	Stiffness of the fork with respect to the shaft, load parallel to shaft
β	Stiffness of the fork with respect to the shaft, thermal loading
γ	The dimensionless value of Δ_x / F_x
σ	Extreme fiber stress in the fork

I. INTRODUCTION

A. Purpose of Project

This project has had the goal of providing scientific data to the Astrionics Laboratory as an aid in the process of achieving an efficient gyro or accelerometer cover design for anticipated temperature and inertia fields. The following section recapitulates the results and conclusions of these efforts in which the structures, materials and design sciences were amalgamated in a carefully integrated program to achieve the project goal. The realization of that goal is substantiated in the five project reports of which this is the last.

The details of this final task appear in the remainder of the report.

B. Project Recapitulation

The project began in November 1965. Initial emphasis was upon determination of fork and shaft temperatures in steady state running, and upon resultant fork and shaft forces and deformations. Later on, the importance of careful measurements of material property data was recognized, and the major emphasis in the latter stages of the project has been upon microplasticity and corrosion investigations. The culmination of all the project efforts is delineated in the design charts for fork proportions contained in this report.

The history of Allied efforts is recalled by duplicating the summaries of the preceding four tasks.

Task I Summary (November 1964-July 1965)

In this thermoelastic investigation of the AMAB-3 accelerometer, a detailed electric analog heat transfer analysis was conducted. Temperature distributions resulting from internal heat generation are described for several conditions. In addition, theoretical internal forces and thermal deformations were computed utilizing data on temperature generated in the stator.

Important conclusions are summarized as follows:

1. The flywheel and end bell are regions of thermal "hot spots".
2. The largest temperature change was found on the 52100 steel shaft while no measureable change could be detected on the beryllium shaft.
3. Higher motor temperatures are to be expected with a steel shaft.
4. Cylinder temperature was found approximately equal to the gas bearing temperature.

5. The flywheel temperature varied, significantly only with the motor temperature.
6. The higher the sleeve temperature the higher the temperature levels found throughout the inner cylinder assembly if the motor temperature remained constant.
7. The thermal resistance of the nitrogen gas gap should have no measureable effect on the temperature distribution.
8. Thermal deformations of 8 microinches may be expected to occur in normal operation.
9. For an air atmosphere for the motor the temperatures in the thermal "hot spots" tend to be lower than for a helium atmosphere for the same motor temperature.
10. For the same power input the air atmosphere produces higher motor temperatures than the helium atmosphere.
11. Temperature differences of the order of 1 F were found between the opposite extremities of the shaft due to the non-symmetrical design using a helium atmosphere.
12. Fabrication tolerance should not affect thermal deformations.

Task II Summary (July 1965-October 1965)

In this thermoelastic investigation of the AB-5 stabilization gyro, a detailed electric analog heat transfer analysis was conducted. Temperature distributions resulting from internal heat generation are described for several conditions. In addition, theoretical internal forces and thermal deformations were computed utilizing data on temperatures generated in the stator. Photothermoelasticity was used to verify the theoretical thermoelastic behavior.

Important conclusions are summarized as follows:

1. The flywheel fabricated from Elkonite should have an insignificant effect on temperature distributions for steady state conditions. However, it should affect the transient state.
2. The flywheel and end ball are regions of thermal "hot spots".
3. The largest temperature change was found on the 52100 steel shaft.
4. High motor temperatures should occur with the steel shaft design with ten watts power input.
5. Cylinder temperature is approximately equal to the gas bearing temperature.

6. The flywheel temperature varies only with the motor temperature.
7. The higher the gas bearing temperature the lower the temperature drop on the shaft if the motor temperature remains constant.
8. The thermal resistance of the nitrogen gas gap would have no measureable effect on the temperature distribution.
9. Thermal deformations in the order of 50 microinches may occur in normal operation.
10. Fabrication tolerances should not affect thermal deformations.
11. Preliminary studies of dimensional instability indicate microstrain and microcreep in components could affect gyro performance.
12. A change in the basic design to a symmetric structure support for the shaft would be expected to reduce the effect of temperature gradients.

Task III Summary (October 1965- November 1965)

Theoretical and experimental temperature investigations were made of the AB-5 gyro and AMAB-3 accelerometer. Thermocouples were located at strategic nodes in the prototype components and temperatures were measured after steady state conditions prevailed. The temperature distributions obtained experimentally, simulating heat generated in the stator with no wheel rotation, were compared with theoretical values obtained from computations employing an analog described in previous reports (Refs. 1, 2).

Important conclusions are summarized as follows:

AB-5 Gyro and AMAB-3 Accelerometer

1. Hot spot exists in the end bell.
2. Cylinder temperature approximately equals gas bearing temperature.
3. Small temperature gradients exist in the prototype.
4. End bell temperature is lower than shaft temperature adjacent to the stator.
5. No appreciable heat flows through the ball bearings.

AMAB-3 Accelerometer

1. No measurable temperature gradient was observed on the shaft.
2. Bearing gas has no measurable effect on temperature distributions.

Task IV Summary (November 1965 - April 1966)

Theoretical and experimental investigations were conducted on the structure and the materials of the first of several redesigns of the AB5-K8 gyro. Shock and temperature loads were considered, and determination was made of the microinch offset yield strength of the beryllium now being used in the gyro.

As a result of the investigation, elementary beam theory was shown to be a reliable procedure for predicting shaft deflections, a simple method of transient heat transfer was shown to have promise in shaft design, and an efficient fork configuration appeared to be achievable using thin, flat members cantilevered from the cover plate. The microinch offset yield strength of S 100 beryllium was at the low end of the range of properties of standard beryllium metal, below that of the high PEL beryllium (I 400), and far below what might be expected of steels.

II. MICROPLASTICITY EXPERIMENTS

A. Introduction

We had previously reported (Reference 1) the low stress level microplastic behavior obtained from a number of tests on one specimen of beryllium, Bendix material specification 450 A Grade A which is equivalent to Brush S 100 material. This particular material had been used in fabricating a number of structural members of the AB50-K8 gyro. Since permanent material displacements in the instrument of the order of one microinch (25 micromm) might have an effect on instrument precision and accuracy, it was appropriate to study the stress magnitudes which would result in permanent strains of the order of 10^{-5} to 10^{-7}.

Tests which were performed on samples of the S 100 material reported here and reported in reference 1, indicated that a stress level of approximately 2000 psi (13.8 N/mm^2) would result in a permanent strain of 1×10^{-6}. (As a matter of identification the stress level which results in a permanent plastic strain of 1×10^{-6} will be called the one microinch offset yield stress (1 MOYS throughout the remainder of this report). A second loading of the same specimen in the reverse direction showed a 1 MOYS value of 1500 psi (10.3 N/mm^2).

It was conceivable that the structural members of the instrument would sustain higher values of stress than the 1 MOYS of S 100 beryllium. We, therefore, initiated a testing program to perform additional tests on S 100 material and to identify other materials which might have higher 1 MOYS values and which would also be suitable for application in the instrument.

The materials tested and reported herein included the following:

1. Beryllium: Bendix Specification 450 A Grade A (Brush S 100)
2. Beryllium: Bendix Specification 450 A Grade D (Brush I 400)
3. Steel: Type 52100
4. Lockalloy: Beryllium-Aluminum Alloy
5. Elkonite: Tungsten-Copper Alloy

The chemical composition of each of these materials and available processing and properties data are given in Appendix I.

B. Testing Procedure

The testing technique employed the standard load-unload procedure either in bending or in compression. For the bending tests an I-beam configuration shown in

Fig. 1 was used, similar to that which was described in Ref. 1 for the S 100 tests. The strains were measured by temperature compensated foil strain gages BLH type FAP-12-12S6 installed on both the compression and tension surfaces of the beam specimen in a full bridge arrangement. These gages have a gage length of 0.125 in. (3.2 mm), are paper backed, and were attached with SR-4 cement. The bending moment was applied by a loading whiffletree which is shown in Figure 2. Compression tests were performed on simple cylindrical specimens between hardened fixed platens in an ARA testing machine.

Two strain measurements were made for each load increment: the strain value at the applied load and the strain reading when the load was removed. From the former a stress-strain curve was obtained and this allowed for a determination of Young's modulus for comparison with published values. We would be assured that the technique was valid if the experimental and published values of Young's modulus were in agreement. The residual plastic strains were determined from the no-load strain readings.

C. Temperature Compensation

Temperature changes of the order of 1F (0.6 K) can result in thermal strain magnitudes in most metals which are five times greater than the microplastic strain values measured here. However, the full bridge strain gage configuration was self temperature compensating for thermal strains providing no varying temperature gradient existed in the specimen and providing that the response of each of the strain gages was the same under changing temperature.

Working in an air conditioned laboratory, we saw no need for using elaborate temperature control procedures in the beam tests aside from shielding the specimens from gross air movements which could result from doors being opened, etc. In every case the strain instrumentation was turned on and allowed to stabilize for at least one hour before the test. We also performed an experiment designed to check the efficiency of our temperature compensation techniques. After a load-unload test on one of the Beryllium I 400 specimens, an additional load-unload test was performed with the same direction of loading using the same stress increments. In this additional test, however, the beryllium test material, having been previously strained, was completely elastic and ideally there should have been no residual plastic strains. Any residual strains which would be observed should be thermal in origin. The test results showed a maximum residual strain of 1.2×10^{-7} and this could be considered the maximum thermal effect in any one test under the conditions of the bending tests.

In the compression experiments a temperature compensating specimen was used and it was placed adjacent to the loaded specimen. The table model ARA testing

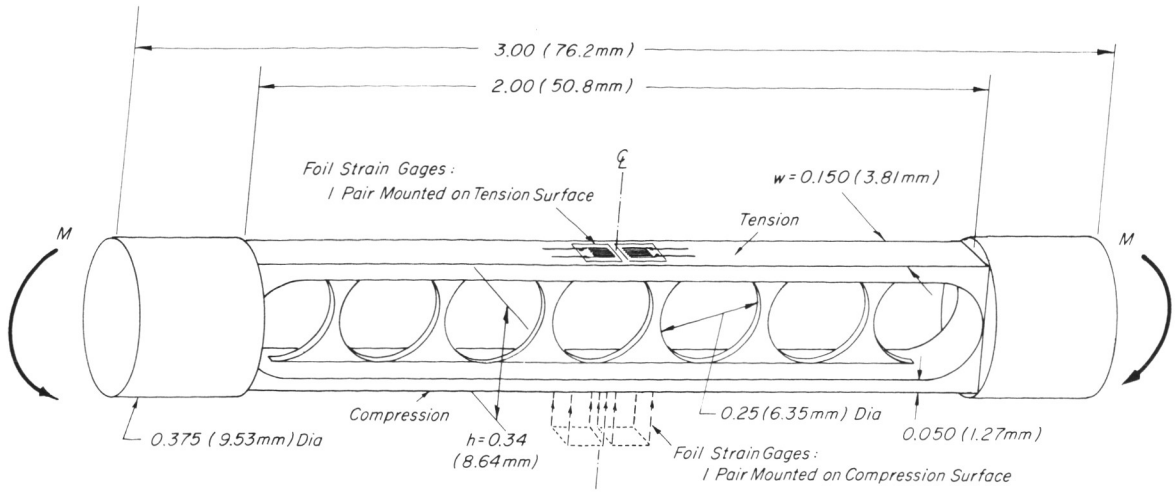

Figure 1 Beam Specimen Configuration

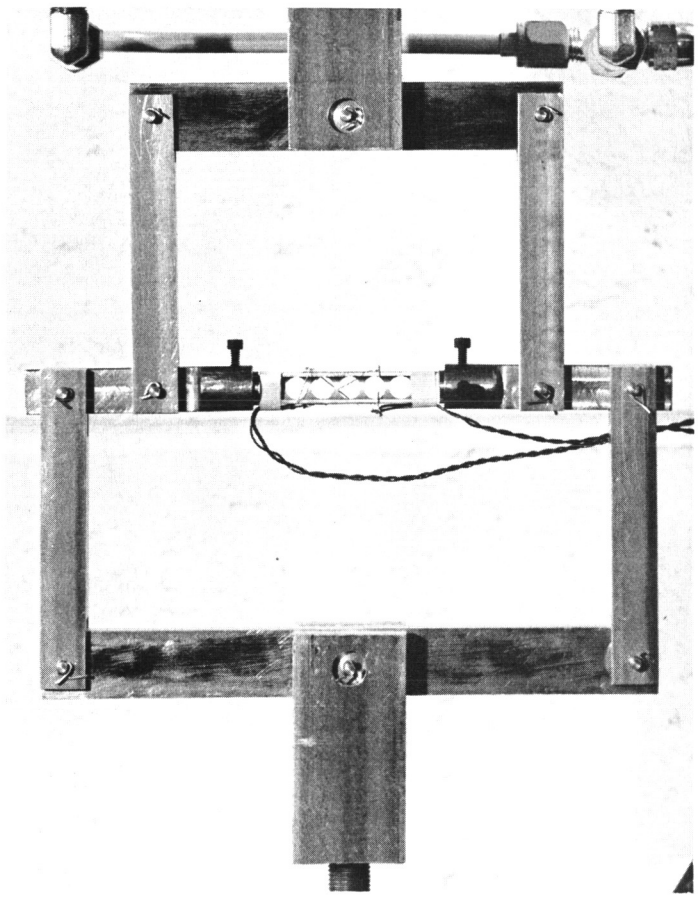

Figure 2 Loading Whiffletree Used to Apply a Pure Bending Moment to Beam Specimens

machine, which we used for the tests, was then enclosed in a plastic tent. The gages were energized and allowed to stabilize for one hour before testing was begun.

D. Beryllium S 100 (Specimen 5-1)

We had previously reported a test program using S 100 beryllium that evaluated the microplastic behavior of two types of beam specimens: a flat and an I-beam configuration. As reported in Ref. 1, the I-beam configuration proved to be more suitable than the simpler flat specimen. An additional I-beam specimen was fabricated of S 100 material and heat treated for stress relief. This specimen was tested in bending in an initial test and the direction of bending was reversed in a second test for an assessment of the micro-Bauschinger effect. The test results shown in Fig. 3 show somewhat higher properties than those reported for a previous specimen in Ref. 1. The 1 MOYS values were 2520 psi (17.3 N/mm^2) initially and 2270 psi (15.6 N/mm^2) on reverse loading. The modulus of elasticity values on the initial test and on reverse reloading are 42.6×10^6 psi (29.4×10^4 N/mm^2) which are within one percent of the previously measured values.

E. Beryllium I 400 (Specimens 6-1 and 6-2)

This powder metallurgy product is characterized by a relatively higher BeO content (5.36%) than the S 100 material (0.83% BeO). The effect of the increased BeO content on the macro-properties is to raise the 0.2% yield strength of beryllium from approximately 30,000 psi (206 N/mm^2) in the S 100 to 68,000 psi (475 N/mm^2) in the I 400 and to raise the tensile strength from 49,000 psi (337 N/mm^2) to 80,000 psi (550 N/mm^2). It was also to be expected that the micro-properties would similarly be affected: the reported 1 MOYS value for the I 400 material, given by Brush Beryllium was 11,400 psi (78 N/mm^2) as compared with our measured values for S 100 of 2,000-2,500 psi (13.8-17.3 N/mm^2).

Two I-beam specimens were machined from 0.375 in. (9.5 mm) diameter rod and stress relieved by holding at 1325 F (993 K) for one hour in vacuum and by furnace cooling to room temperature. Each specimen was subjected to a load-unload bending test using 500 psi (3.44 N/mm^2) stress increments. Then the direction of bending was reversed and the test was repeated. The second loading in the reverse direction allowed for an assessment of the micro-Bauschinger effect. In the Bauschinger effect, the result of plastic deformation in one direction of loading is to lower the yield stress in the opposite direction. On the microscale, the effect is similar, in that microplastic deformation in one direction lowers the 1 MOYS in the opposite direction.

Strain data were obtained at load and after unloading for each stress increment. The 1 MOYS values were determined from the unload strain data. The load strain data were used to obtain Young's Modulus. This paramenter is a sensitive indicator of the proper operation of the technique when the experimental values are compared with the published values.

Shown in Fig. 4 are the stress-residual plastic strain data for each of the I-400 specimens in the initial loading and the first reversal. The 1 MOYS values on initial loading averaged 7,000 psi (48.2 N/mm^2). As shown in the figure there is a marked micro-Bauschinger effect in this material with large reductions in the 1 MOYS to 3,350 psi (23.1 N/mm^2) and 4,300 psi (29.6 N/mm^2) in the two specimens respectively in the first reversal. On the basis of our previous micro-Bauschinger effect experiments with S 100 beryllium, we would not expect any further reduction in the 1 MOYS with subsequent load reversals but rather a slight increase.

F. Fine Structure of Microplastic Strains in Beryllium S 100 and I 400

In preparing Figs. 3 and 4 a smooth curve was fitted by eye to the individual data points to give a conventional representation to the data. The possibility exists, however, that the scatter of the data around the smoothed curve is not a result of random errors in the instrumentation but may be representative of the microplastic yielding phenomena. The possibility exists that for plastic strains less than 4×10^{-6} there is non-uniform yielding. Hence the discontinuous dashed line connecting the data points may be more representative.

As an explanation, it is appropriate to consider the sensitivity of the measurement in terms of actual displacement in the lattice. One unit on the strain read-out device used in these experiments is equivalent to an average strain of 2.5×10^{-7} on the specimen. The elongation of a 0.125 in. (3.2 mm) strain gage of the type employed in this study under this strain value is of the order of 3.1×10^{-8} in (7.9×10^{-7} mm). In beryllium one atomic spacing is of the order of 1.2×10^{-8} in (3.0×10^{-7} mm). Hence a strain variation of the order of 2.5×10^{-7} around the smoothed curve in the figure represents an actual variation in deformation of less than 3 atomic spacings. If in a given increment of load there is a dislocation slip-stick motion with variation in dislocation displacement of 3 atomic spacings, the results we observe with the beryllium are reasonable.

G. Type 52100 Steel (Specimens 7-1 and 7-2)

Two beam type specimens, similar to that shown in Fig. 1 were rough machined out of annealed bar stock and heat treated to a hardness of Rockwell C63-64. After

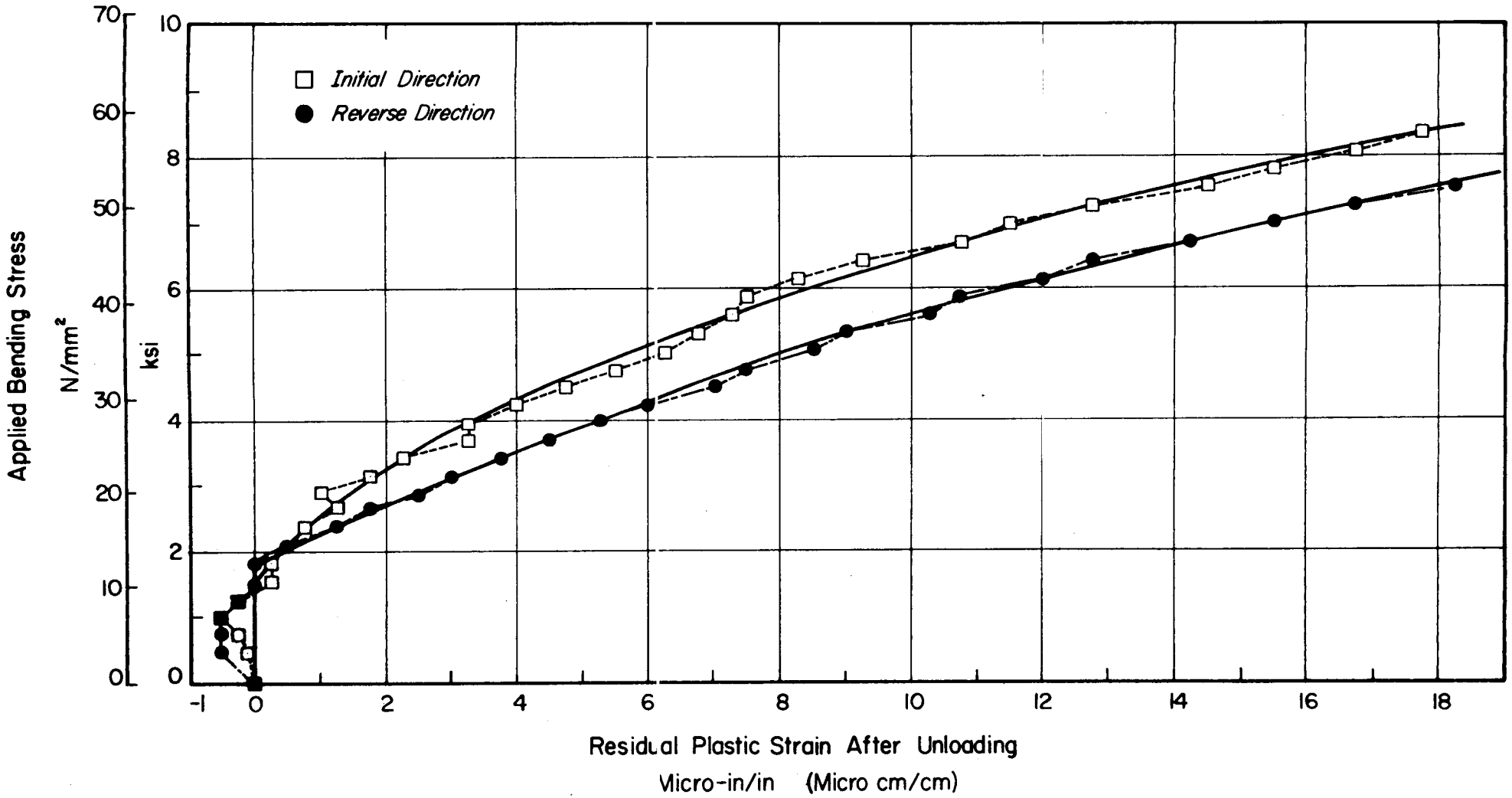

Figure 3 Microplastic Strains from Bending Tests on S100 Beryllium Showing the Micro-Bauschinger Effect

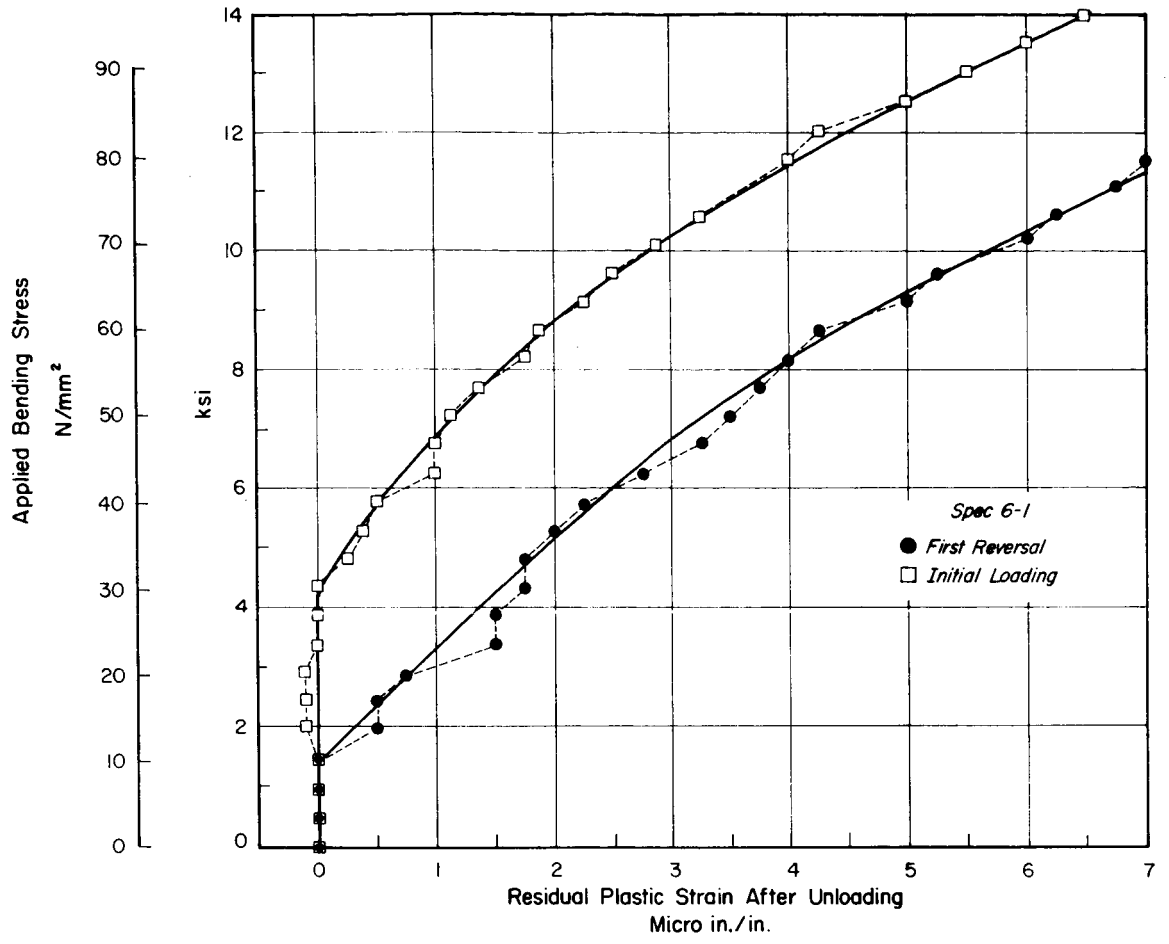

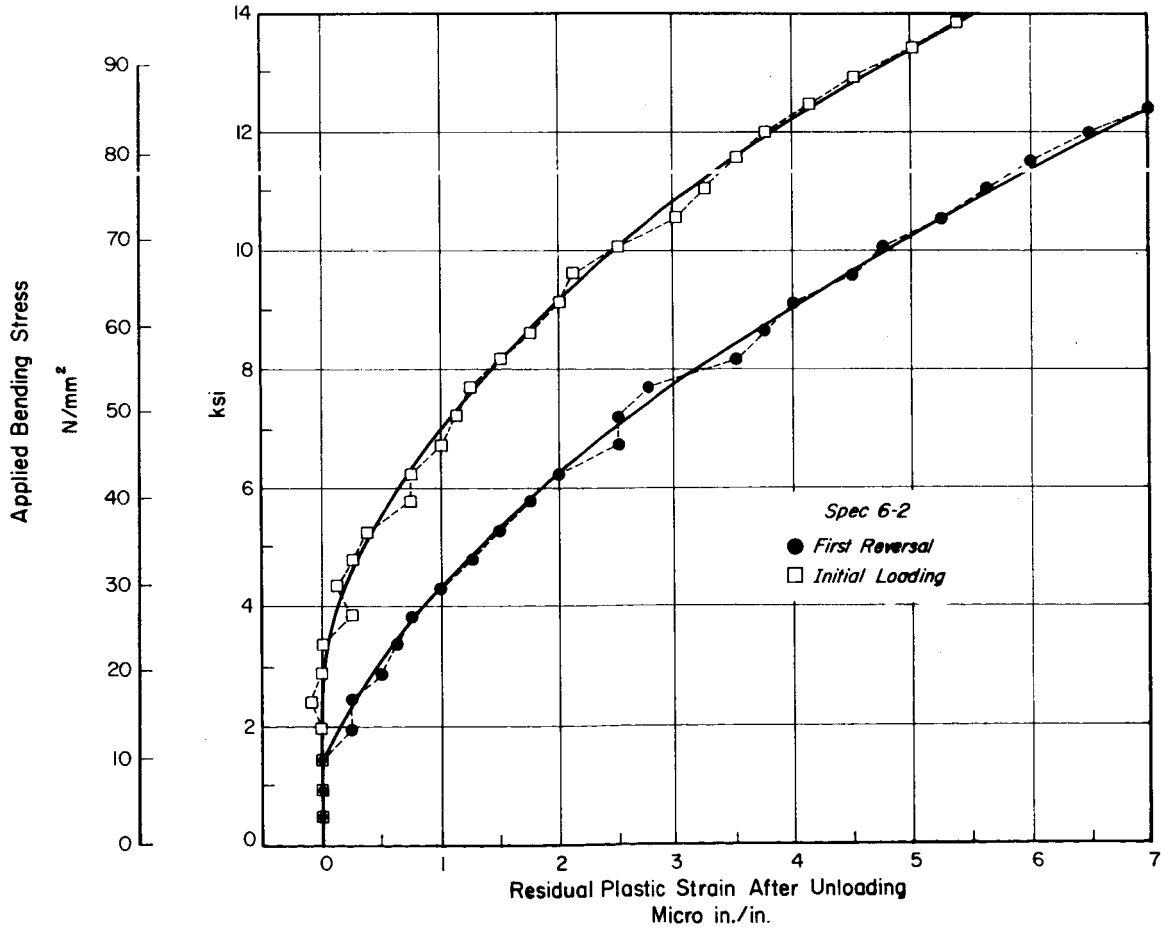

Figure 4 Microplastic Strains from Bending Tests on I 400, High BeO Content Beryllium Showing the Micro-Bauschinger Effect

finish grinding, the specimens were stabilized by thermal cycling between 350F (450 K) and -100F (199 K) for several cycles. The details of the heat treatment are given in Appendix I. Foil strain gages BLH type FAP-12-12S6, similar to those used on the beryllium specimens were applied to both flange surfaces and connected in a full bridge arrangement.

Specimen 7-1 was tested in bending using the arrangement shown in Fig. 2 with the load-unload procedure. Loading to a maximum stress level of 29,400 psi (196 N/mm^2) presented indications of negative residual strains as shown in Fig. 5. Testing was discontinued for approximately an hour and the test was repeated this time to a maximum stress level of 58,800 psi (405 N/mm^2). Again the residual strains were negative as shown in Fig. 5. Negative strain results have been observed previously in steel by Reichenbach, Brown, and Russell(2), by Jennings (3) and others using strain gages, however, in each case the results have been attributed to effects in the strain gages or to the bonding technique rather than to the material itself. The modulus of elasticity value obtained from the loading strains was found to be 29.5×10^6 psi (20.3×10^4 N/mm^2) in both experiments, which is in agreement with the published values for this material. This result seemed to indicate that there was no gross malfunction of the strain gages.

We believed at the time that the negative strain results could arise from causes other than the material itself or the strain gages and that these effects might be associated with complex stress interactions in the perforated webs. To test this latter possibility the second I-beam configuration specimen 7-2 was loaded in compression. One strain gage on each flange was used for measuring the strains. The previously tested specimen was used for temperature compensation with all gages in both specimens connected in a full bridge. In this case, however, only two of the gages in the bridge were active. The specimen was loaded to a stress level of approximately 115,000 psi (792 N/mm^2) and as the results given in Fig. 6 indicate, negative strain values resulted. On this basis we could only conclude that the results were not specifically due to the configuration but were due to the material or that they arose in the measurement system. Although the other workers (Refs. 2 and 3) have concluded that such effects are due to the strain gages, conclusive evidence of this has not been presented; rather the judgment has been based upon statistical evidence rather than a clear demonstration of cause and effect.

H. Lockalloy (Specimens 8-1 and 8-2)

As shown in Appendix 1, Lockalloy is an aluminum-beryllium alloy containing approximately 62 percent beryllium and 38 percent aluminum. Two specimens,

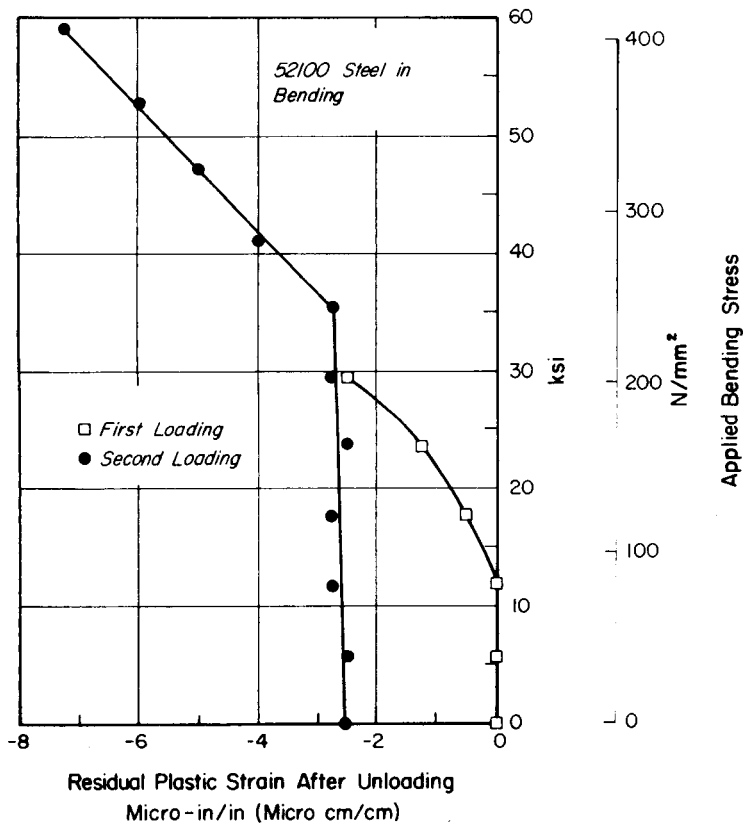

Figure 5 Microplastic Strains from Bending Tests on Type 52100 Steel, Heat Treated and Stabilized

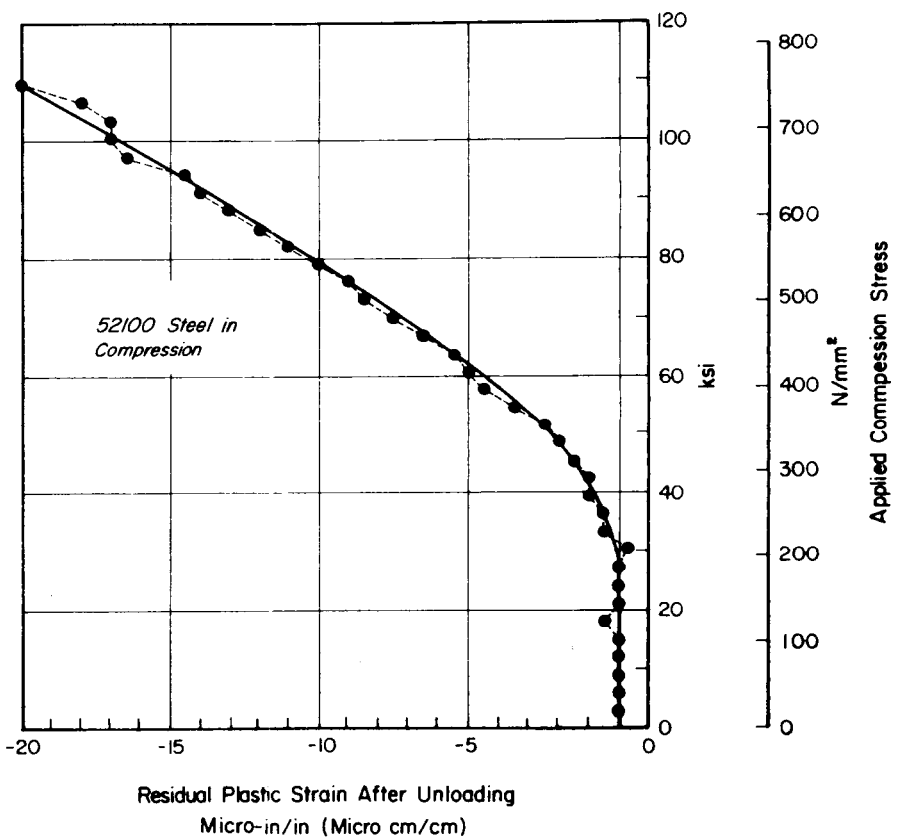

Figure 6 Microplastic Strains from Compression Tests on Type 52100 Steel, Heat Treated and Stabilized

each 0.5 inches (12.7 mm) in diameter and two inches (50.8 mm) long were machined from nominal 0.50 inch (12.7 mm) diameter rod. Pairs of BLH FAP-12-12S6 foil strain gages were applied 180° apart at the center of each of the specimens. Specimen 8-1 served for temperature compensation while specimen 8-2 was tested using the load-unload procedure.

The microplastic compression strains for Lockalloy, shown in Fig. 7 indicate a value of the 1 MOYS of approximately 6,500 psi (44.8 N/mm^2) which is comparable with the value for I-400 beryllium. Young's modulus value obtained from the load strain values was 31.6×10^6 psi (21.8×10^4 N/mm^2).

I. Elkonite (Specimen 9-1)

An I-beam specimen was machined from bar stock of this alloy of copper (28%) - nickel (3%) -tungsten (69%) and stress relieved after machining at 600F (589 K) for 2 hours in an inert atmosphere. The specimen was similar to that shown in Fig. 1, however, a solid web rather than a perforated web was used.

The specimen was tested in bending in one direction and then a second test was performed in the opposite direction. The results, shown in Fig. 8, are interesting in that there appears to be a negligible micro-Bauschinger effect with the Elkonite material with both values of the 1 MOYS at approximately 11,000 psi (76 N/mm^2). In this respect this material differs from the other tested. Young's modulus as obtained from the load-strain values was 31.8×10^6 psi (21.9×10^4 N/mm^2) on the initial loading.

Summary of Results

A summary of the microplastic strain data for each of the materials tested is given in Table 1.

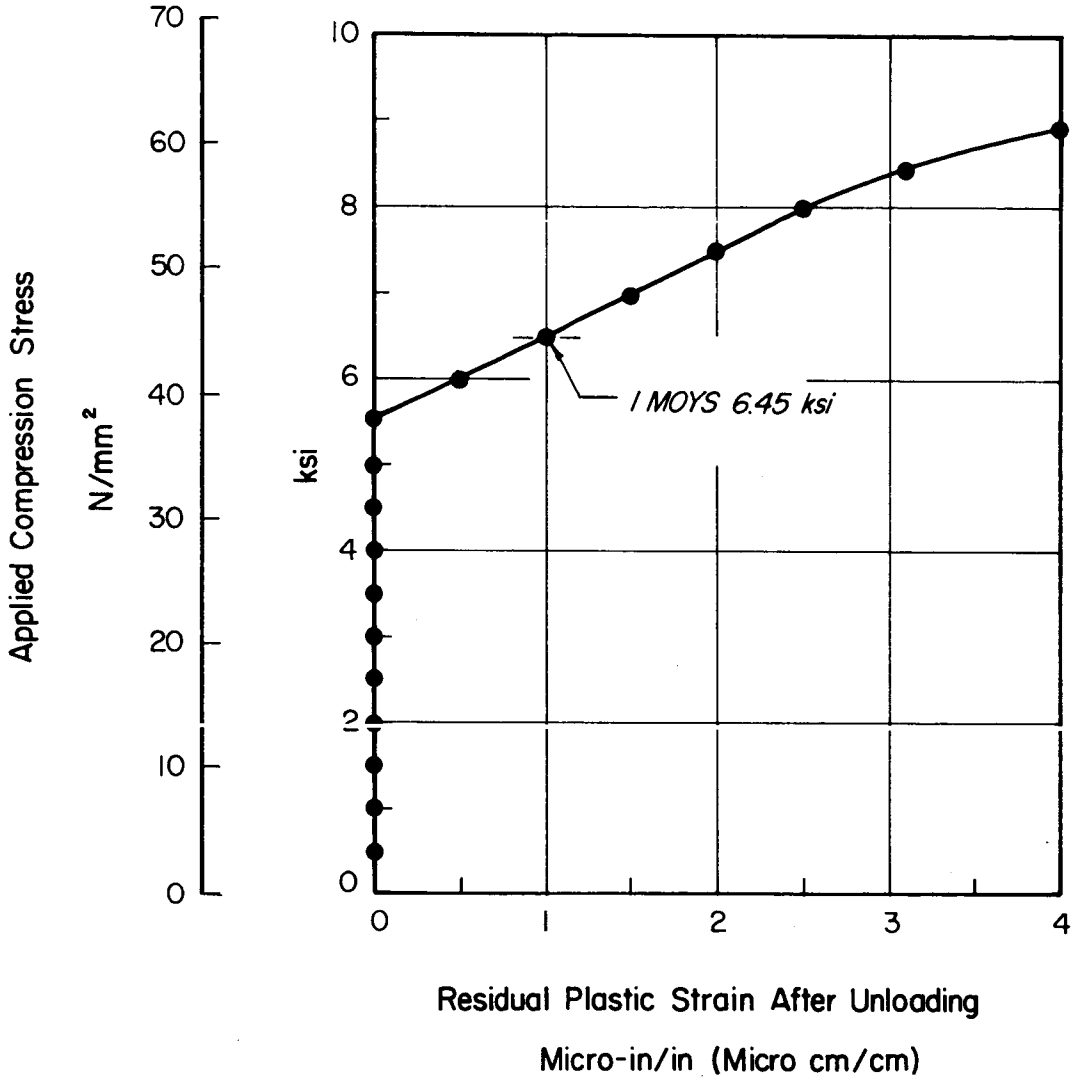

Figure 7 Microplastic Strains from Compression Tests on Lockalloy, Beryllium-Aluminum Alloy

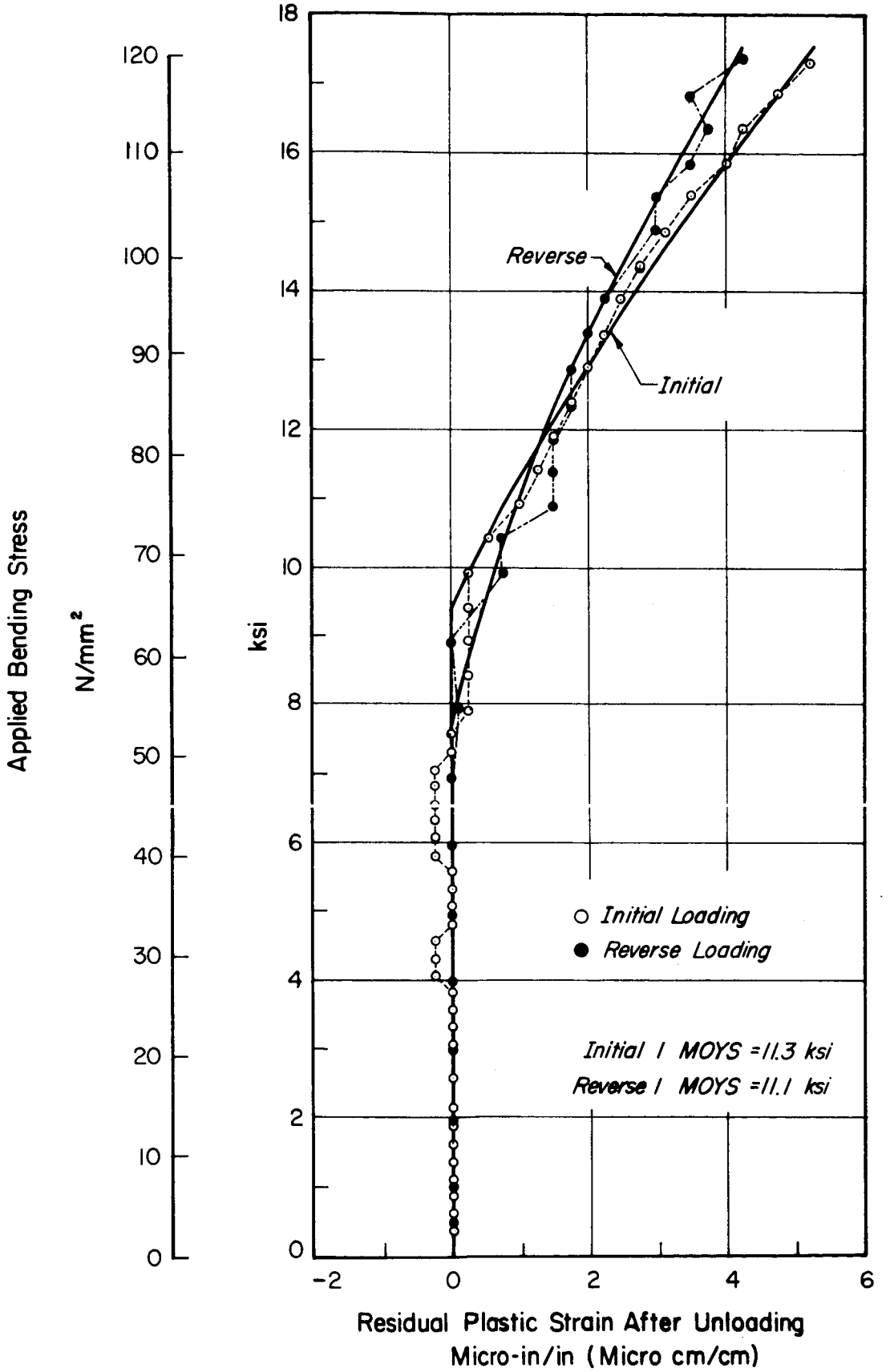

Figure 8. Microplastic Strains from Bending Tests on Elkonite, Tungsten-Copper Alloy

Table 1 Microplastic Data Summary

Specimen Material	Specimen No.	Loading Direction	Modulus of Elasticity 10^6 psi	Modulus of Elasticity 10^4 N/mm^2	1 Microinch Offset Yield Strength psi	1 Microinch Offset Yield Strength N/mm^2	Stress for less than 0.25×10^{-6} strain psi	Stress for less than 0.25×10^{-6} strain N/mm^2
Beryllium S 100	1-2*	Initial	43.1	29.7	2010	13.8	960	6.7
		1st Reverse	43.1	29.7	1490	10.2	700	4.8
		2nd Reverse	-	-	1300	8.9	400	2.8
		3rd Reverse	-	-	1490	10.2	700	4.8
Beryllium S 100	5-1	Initial	42.7	29.4	2520	17.3	1500	10.3
		1st Reverse	42.5	29.3	2270	15.6	1820	12.5
Beryllium I 400	6-1	Initial	43.8	30.2	6900	47.5	4170	28.7
		1st Reverse	43.0	29.6	3350	23.1	1330	9.2
	6-2	Initial	44.5	30.6	7000	48.2	3000	20.7
		1st Reverse	43.6	30.0	4300	29.6	1370	9.4
Steel 52100	7-1	Initial	29.5	20.3	21800**	150.0	10200**	70.3
	7-2	Initial***	-	-	41200**	284.0	29000**	200.0
Lockalloy	8-2	Initial***	31.6	21.8	6450	44.4	5500	37.9
Elkonite	9-1	Initial	31.8	21.9	11300	77.8	9400	64.8
		1st Reverse	31.2	21.5	11100	76.4	7600	52.4

* Data from Ref. 1.

** Negative residual plastic strains.

*** Compression Loading; all others tested in bending.

III. METALLURGICAL INVESTIGATIONS

A. Introduction

Some preliminary optical and electron metallographic studies were made on beryllium to establish the value of such studies in explaining the microdeformation behavior of these materials under stress. These studies involved principally (1) the definition of the overall metallographic structure by optical metallography, (2) the study of dislocation positions and movement using etch pit techniques and electron metallography, and (3) temperature-humidity corrosion tests.

B. Materials

The materials studied were:

QMV Beryllium Rod - Brush S 100 (Low Microinch Offset Yield Strength)
QMV Beryllium Rod - Brush I 400 (High " " " ")
Berylco Rod - Lockalloy (Be - 38Al)

Chemical composition and treatments of these materials are given in Appendix I.

C. Optical Metallography

The essential difference between the S 100 and I 400 beryllium is in the BeO content. The higher properties of the I 400 are purported to be the result of the higher BeO content. Figs. 9 and 10 show the BeO particles in unetched samples at 750X. BeO particle counts were made using a 3" x 4" plane section at 750X. On the basis of these counts the number of particles per square inch at 750X was found to be 40 for the S 100 and 191 for the I 400.

Studies were also made on the bend test specimens of S 100 beryllium. The specimen material as received has the structure shown in Fig. 11 indicating no twinning. After straining plastically to about 10 micro-in/in (10 micro cm/cm) the structure is as shown in Fig. 12 indicating some twinning. For dislocation studies this strained material was vacuum annealed for 8 3/4hrs. at 2000 F (1370 K) and its structure shows the absence of twins and somewhat coarser grains (Fig. 13).

The microstructure of I 400 Beryllium is shown in Fig. 14. The microstructure of Lockalloy is shown in Fig. 15. The electropolishing solution used with the Lockalloy follows:

700 Ml	Ethanol (95%)
100 Ml	Butoxyl Ethanol
200 Ml	Perchloric Acid (30%)

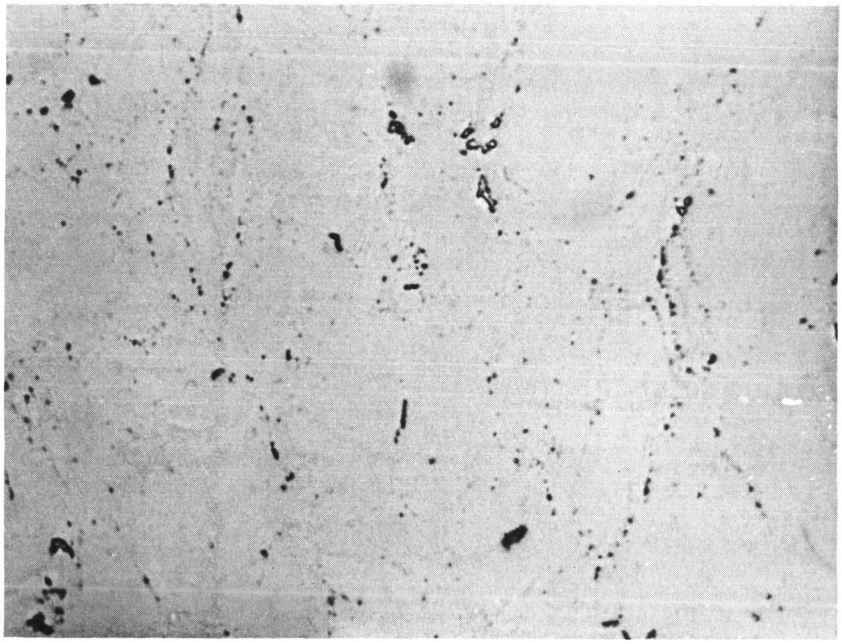

Unetched Mag. 750 X

Figure 9 BeO Distribution in S 100 Beryllium

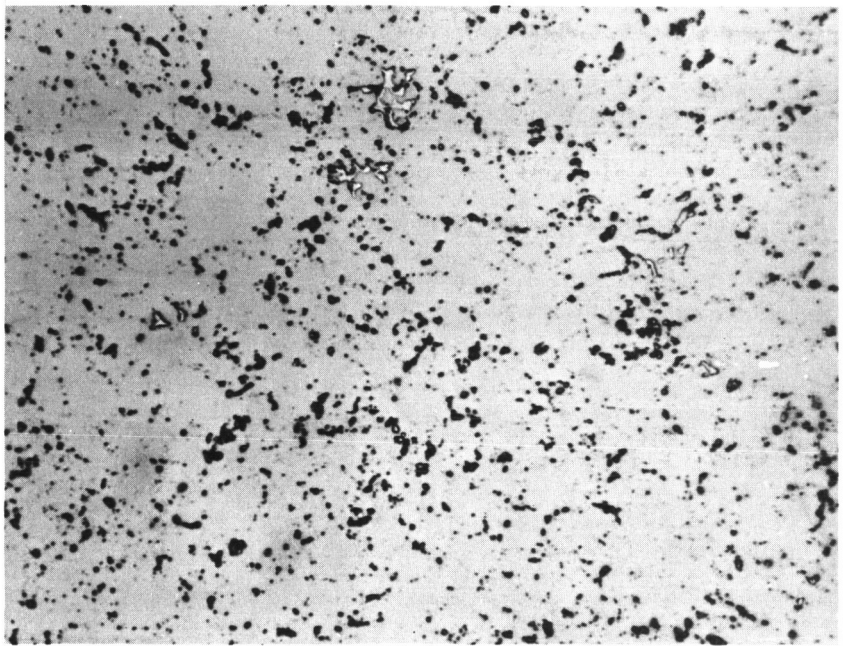

Unetched Mag. 750 X

Figure 10 BeO Distribution in I 400 Beryllium

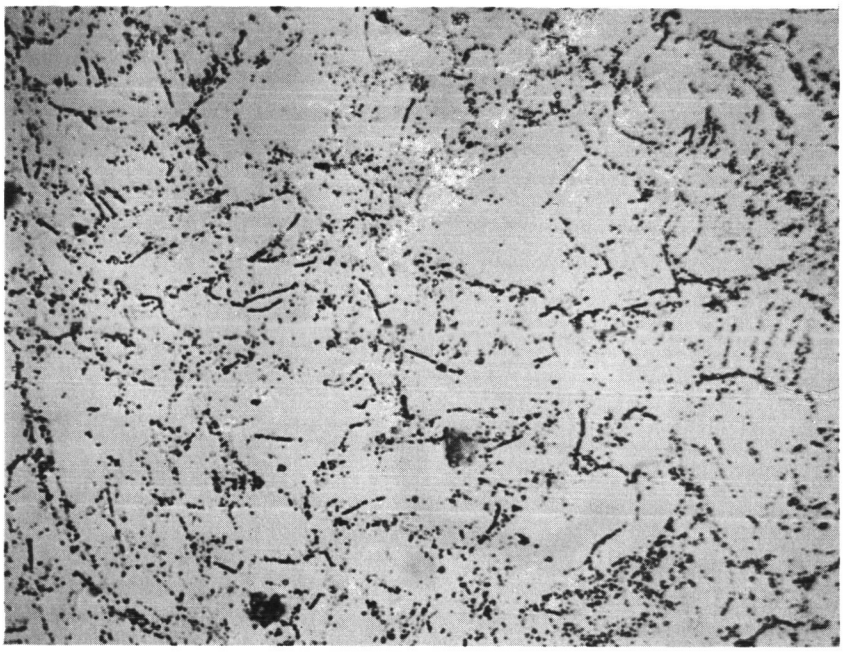

Mag. 750 X

Figure 11 Microstructure of S 100 Beryllium As Received

Polarized Light Mag. 250 X

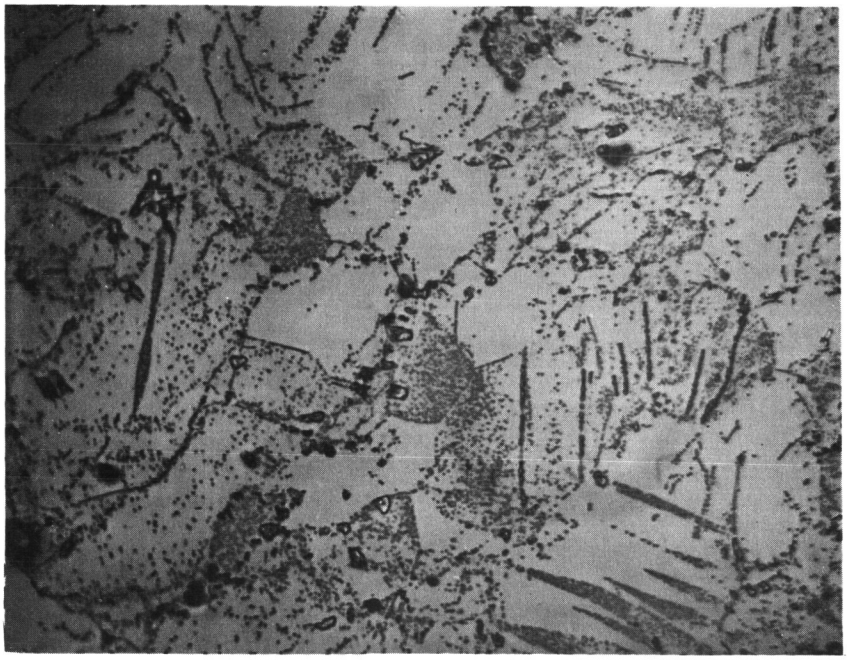

Mag. 750 X

Figure 12 Microstructure of S 100 Beryllium Bend Specimen Surface after 10 microinch/inch Plastic Strain

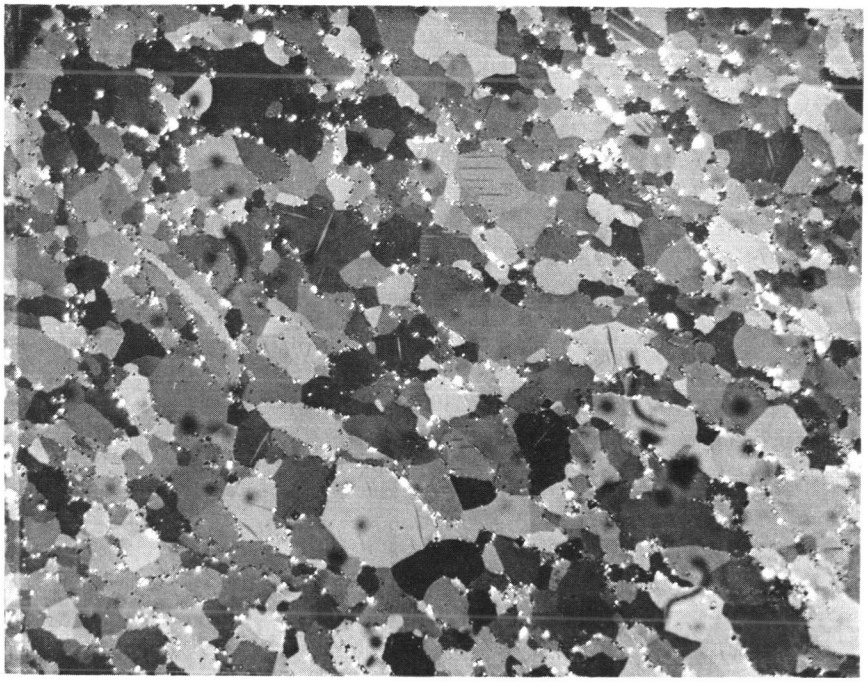

Polarized Light Mag. 250 X

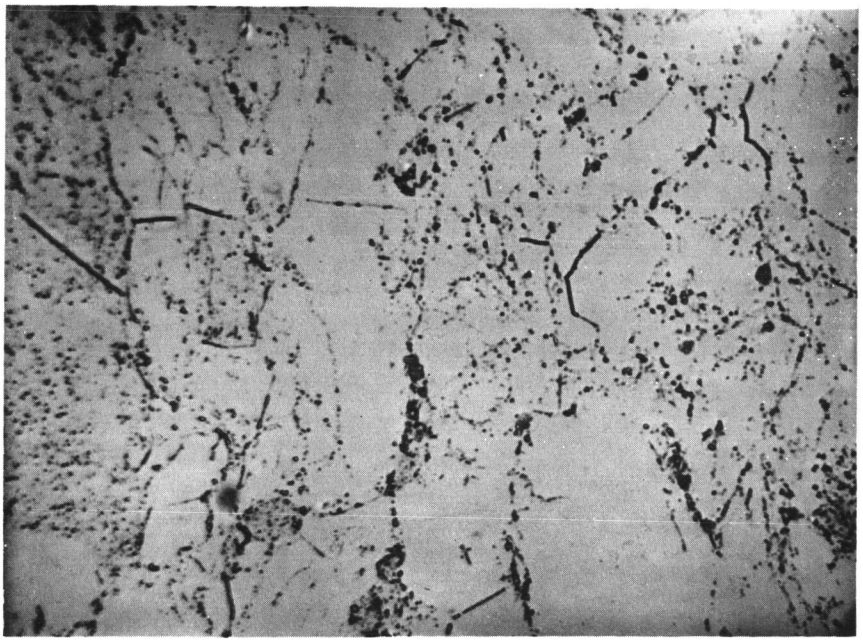

Mag. 750 X

Figure 13 Microstructure of S 100 Beryllium Bend Specimen Surface after 10 microinch/inch Plastic Strain Followed by Vacuum Annealing at 2000 F (1370 K) for 8 3/4 Hours

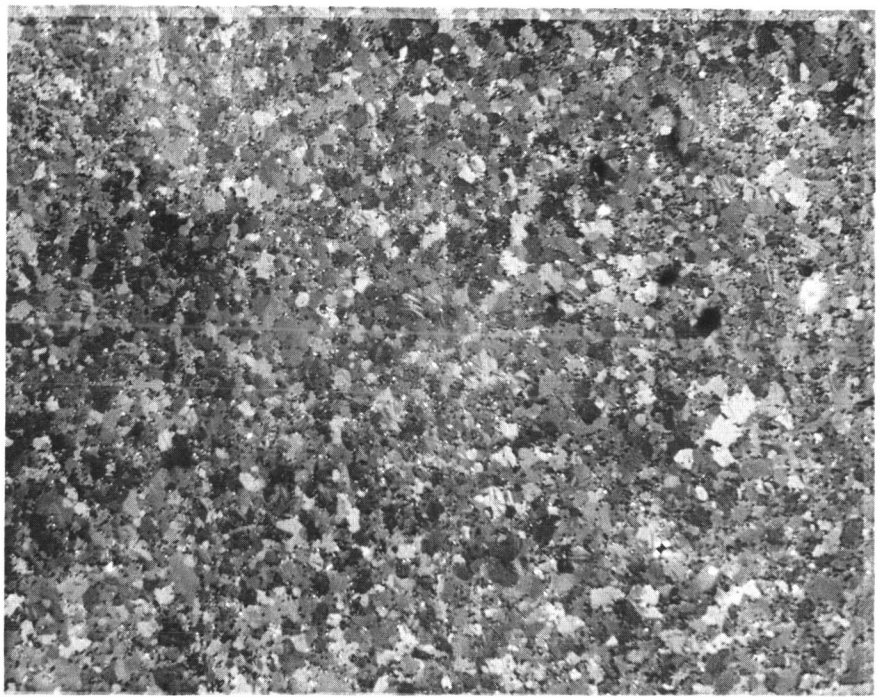

Polarized Light Mag. 250X

Figure 14 Microstructure of I 400 Beryllium As Received

Longitudinal Mag. 750 X

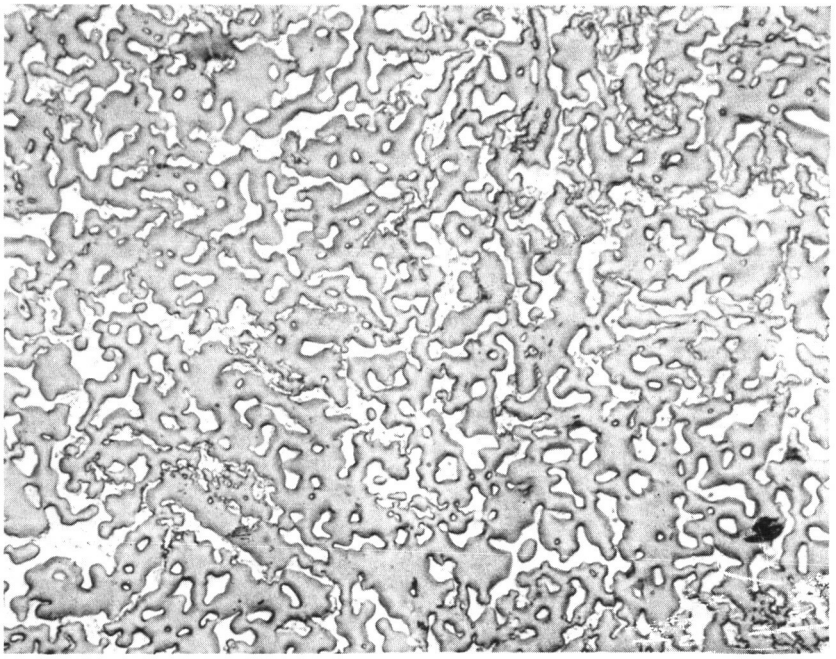

Transverse Mag. 750 X

Figure 15 Microstructure of Lockalloy (Be-38Al)

D. Electron Metallography

To investigate the possible correlation between microstrain and dislocation density in beryllium the electron microscope was used in conjunction with etch pitting technique.

The procedure for producing etch pits at dislocation sites and "decorating" them with copper for observation with the electron microscope was as follows:

1. Electropolishing.

   Electrolyte: 750 Ml ethylene glycol
   15 Ml nitric acid
   15 Ml sulfuric acid
   15 Ml hydrochloric acid

   Polishing Time - 2 minutes

   Polishing Voltage - 16 volts

   Immediately rinse specimen in ethyl alcohol, followed by isopropanol.

2. Copper Sulfate Solution.

   100 Mg cupric sulfate
   200 Ml distilled water

   Immerse specimen for 15-30 seconds. Rinse in distilled water followed by isopropanol.

Fig. 16 shows the etch pit pattern of dislocation sites for the S 100 beryllium in the as received condition. Fig. 17 shows the corresponding pattern for the S 100 beryllium test specimen after plastic straining 10 micro in/in (10 micro cm/cm) indicating slightly greater density. Since both of these specimens showed rather high density, it seemed advisable to establish a base pattern for fully annealed beryllium. A much reduced dislocation density is shown in Fig. 18 for a sample vacuum annealed at 2000 F (1370 K) for 8 3/4 hours.

The average etch pit count for a typical square inch on the 7500X micrographs for these three conditions of S 100 is as follows:

Condition	Number of Etch Pits
Strained 10 micro in/in (10 micro cm/cm) in Bending	178
As Received	150
Annealed 2000 F (1370 K) 8 3/4 hours	30

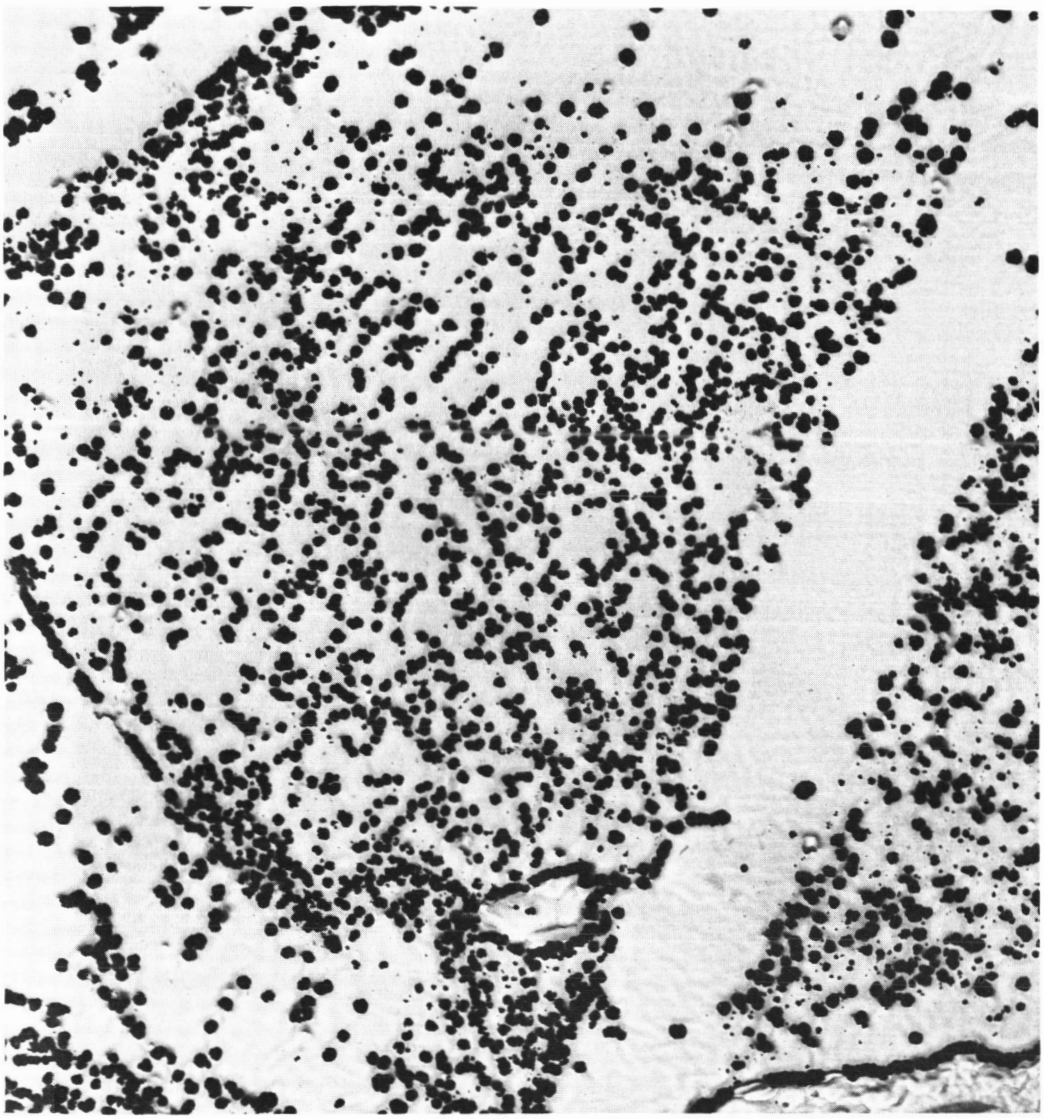

Mag. 7500X

Figure 16 Electron Micrograph Showing Etch Pits in S 100 Beryllium As Received

Mag. 7500X

Figure 17 Electron Micrograph Showing Etch Pits in S 100 Beryllium After Plastic Straining 10 microinch/inch

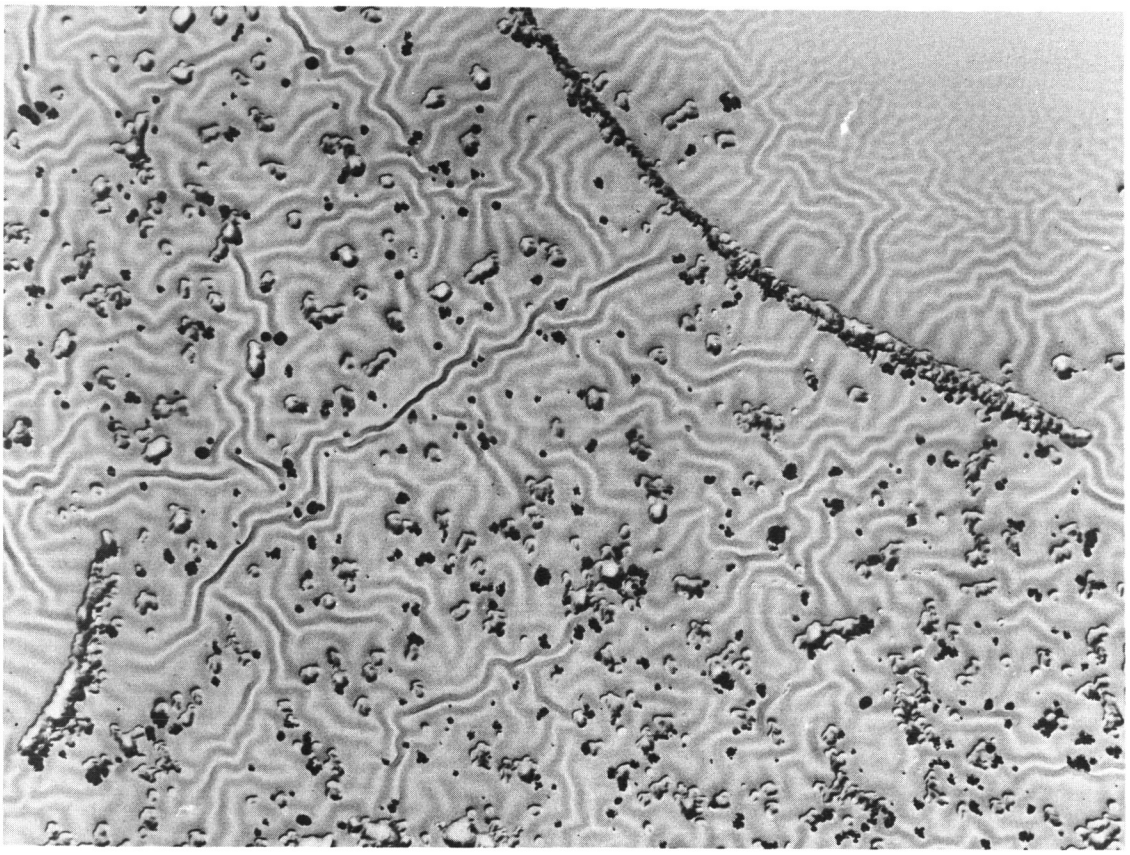

Mag. 7500 X

Figure 18 Electron Micrograph Showing Etch Pits in S 100 Beryllium After 2000 F (1370 K), 8 3/4 Hour Anneal

Attempts to produce etch pits in the I 400 and Lockalloy using the same procedure as for the S 100 were unsuccessful. Development of suitable techniques for these materials was not included in this phase of the program.

E. Corrosion Tests

In view of comments concerning the observance of pitting only on I 400 material after temperature-humidity tests (MIL-E-5272 c), samples of S 100, I 400, and Lockalloy were subjected to this test simultaneously in the same chamber. The details of the test observations are given in Appendix II.

It appears from this simultaneous exposure that surface effects appear at about the same time and develop equally fast in all three materials. The specimens after test are shown in Fig. 19. White corrosion products are present at various locations on all specimens. In some locations pitting is present under the corrosion product deposits.

X-ray diffraction studies at Oak Ridge (4) on similar white deposits tentatively indicated that they are dehydrated beryllium oxide and/or beryllium hydroxide caused by the slow hydrolysis of beryllium carbide inclusions.

F. Discussion

The overall metallographic structures determined by optical metallography appeared normal. The BeO content was reflected in about the same percentage indicated by chemical analysis. Twinning resulting from small microstrains was observed. The I 400 material had a finer grain size in the as received condition than the S 100, which factor should be considered in more exhaustive studies of these materials.

It is apparent that the electron microscope combined with etch pitting techniques can be used to point out reasons for differences in the plastic behavior of beryllium under low stress. The observation of dislocations by these techniques would contribute to the evaluation of metallographic structures most conducive to the development of higher one microinch offset yield stress in instrument materials. It was observed that etching and decorating procedures may have to be developed for various beryllium materials. A possible explanation of the difficulty in producing etch pits in the I 400 is that most of the dislocations may be located close to the BeO particles rather than in the matrix beryllium.

The temperature humidity test was very limited but it seems likely that if critical beryllium gyroscope components are, in fact, subjected to the environment used in this test, some difficulties should be anticipated from the corrosion product and/or the pitting. The behavior of the three materials tested appear to be similar.

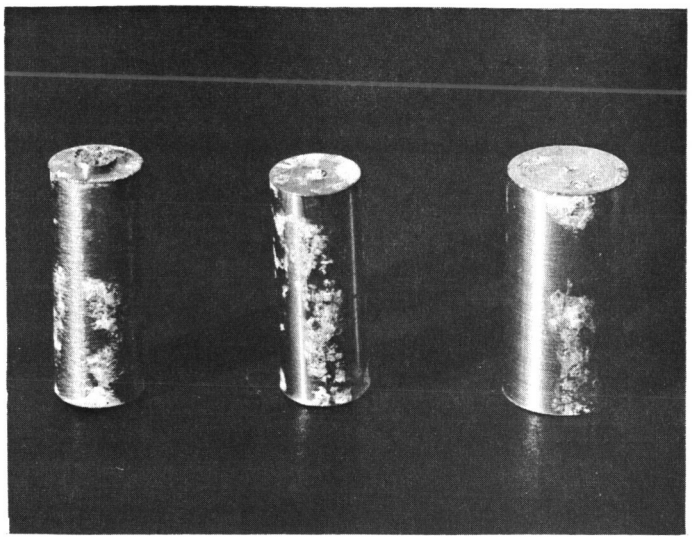

Mag. 1 1/2 X

S 100 I 400 Lockalloy

General Appearance of Specimens

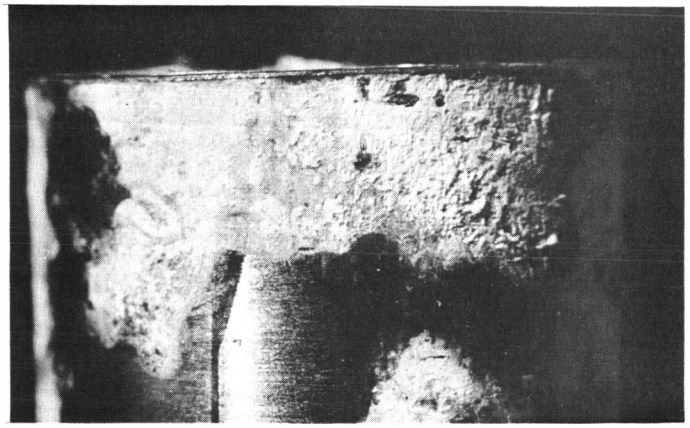

Mag. 10 X

I 400

White Corrosion Products

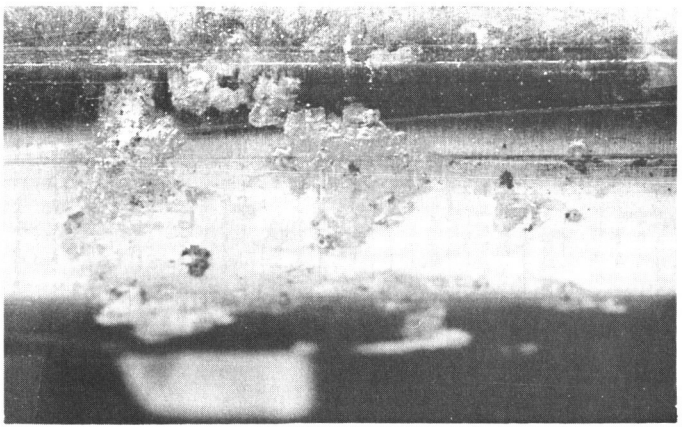

Mag. 10 X

I 400

Pits Below White Corrosion Products

Figure 19 Beryllium Specimens after Temperature Humidity Tests

IV. FORK OPTIMIZATION

A. Introduction

The first requirement for the design of fork is that the transverse rigidities in the directions of the principal axes should be equal. Satisfying this condition, the fork should sustain the thermal loading caused by a given amount of temperature differential between the hot shaft and the cool fork. Also, the fork needs to take a specified amount of quasi-dynamical impact force applied either longitudinally or transversely.

The structure of fork and shaft is assumed as shown in Fig. 20. The internal forces acting on the ends of fork are shown in Fig. 21. The deflections of the structure caused by the applied loads are shown in the same figure. The fork design is then optimized on the basis of this structure.

B. Fork Design for Equal Rigidities

The deflection at point a in the x direction (Fig. 21a) due to load F_x is

$$\Delta_x = \frac{\ell_f^2}{EI_y} \left(\frac{\ell_f}{3} P - \frac{1}{2} M \right) \tag{1}$$

where P and M are the internal forces shown in Fig. 21a. From equations of section C on pg. 18 in Ref. 1,

$$P = \frac{\bar{r}_x}{2} \tag{2}$$

and

$$M = \frac{\ell_s^2 \left(\frac{\theta}{p}\right)_f F_x}{2\left[\left(\frac{\theta}{m}\right)_f + \left(\frac{\theta}{m}\right)_c\right] \ell_s^2 + 8 \left(\frac{\delta}{S}\right)_{sh}} \tag{3}$$

Substituting into Eq. (1) leads to the following equation.

$$\frac{\Delta_x}{F_x} = \frac{\ell_f^3}{6EI_y} \gamma \tag{4}$$

where

$$\gamma = 1 - \frac{3\ell_s^2 \left(\frac{\theta}{p}\right)_f}{2\left[\left(\frac{\theta}{m}\right)_f + \left(\frac{\theta}{m}\right)_c\right] \ell_s^2 + 8 \left(\frac{\delta}{S}\right)_{sh}} \cdot \frac{1}{\ell_f} \tag{5}$$

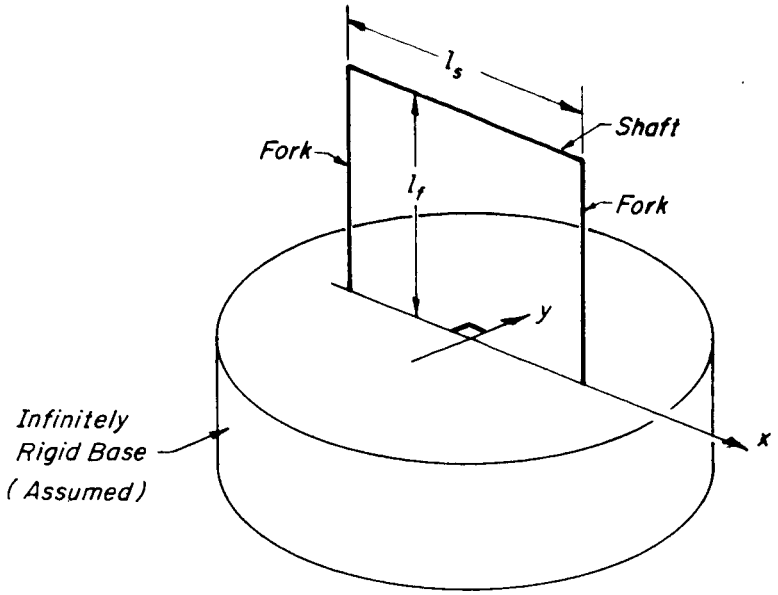

Figure 20 Fork and Shaft

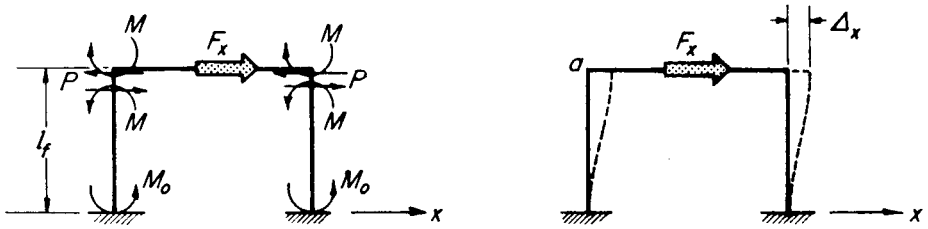

Fig. 21(a)

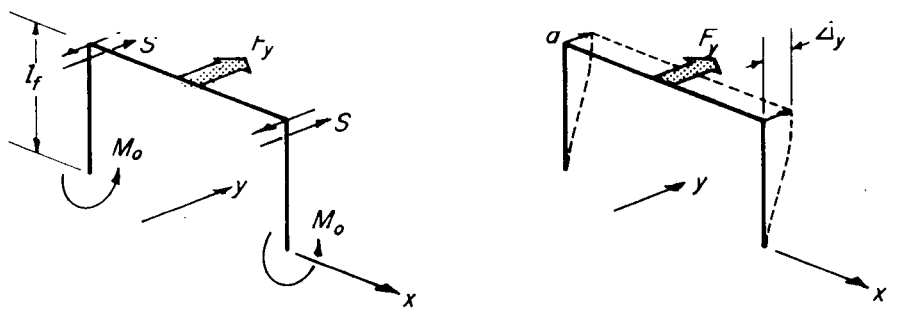

Fig. 21(b)

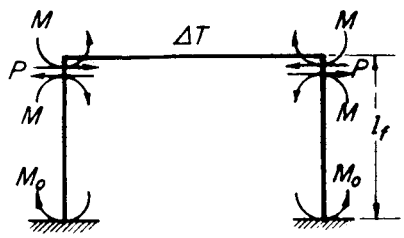

Fig. 21(c)

Figure 21 The Force System in both Fork and Shaft
(a) External force in longitudinal direction
(b) External force in transverse direction
(c) Temperature load

Let

$$\left(\frac{\theta}{p}\right)_f = \frac{\ell_f^2}{2E_f I_f}$$

$$\left(\frac{\theta}{m}\right)_f = \frac{\ell_f}{E_f I_f} \qquad (6)$$

$$\left(\frac{\theta}{m}\right)_c = \frac{c\ell_f}{E_f I_f}$$

$$\left(\frac{\delta}{S}\right)_{sh} = \frac{\ell_s^3}{24 E_s I_s}$$

Here, I_s indicates the effective moment of inertia of the shaft whose value is very close to I_1 in this particular case. Then, by substituting Eqs. (6) into Eq. (5), the expression for γ takes the form

$$\gamma = 1 - \frac{9}{2} \frac{1}{6(1+c) + \beta_1} \qquad (7)$$

where

$$\beta_1 = \frac{E_f \ell_s I_f}{E_s \ell_f I_s} \qquad (8)$$

The deflection at point a in the y direction (Fig. 21b)

$$\Delta_y = \frac{\ell_f^3}{3EI_x} S \qquad (9)$$

where S is the internal force shown in Fig. 21b. As mentioned in Ref. 1

$$S = \frac{F_y}{2} \qquad (10)$$

Then, from Eq. (9)

$$\frac{\Delta_y}{F_y} = \frac{\ell_f^3}{6EI_x} \qquad (11)$$

The condition of equal rigidities requires

$$\frac{\Delta_x}{F_x} = \frac{\Delta_y}{F_y} \tag{12}$$

Using this equation together with Eqs. (4) and (11) the following relation between b and h is obtained,

$$h = \gamma^{1/2} b \tag{13}$$

Thus, to obtain equal rigidities for the fork, the dimension of its cross section must satisfy the above equation.

C. Fork Dimension Versus the Applied Force Parallel to the Shaft

From Eqs. (3) and (6) the expression for M (Fig. 21a) is derived as

$$M = \frac{F_x}{2} \ell_f \frac{3}{6 (1 + c) + \beta_1} \tag{14}$$

As seen from Fig. 21a, the moment M_o is

$$M_o = \frac{1}{2} F_x \ell_f - M \tag{15}$$

or

$$M_o = \frac{F_x}{2} \ell_f \left[1 - \frac{3}{6 (1 + c) + \beta_1} \right] \tag{16}$$

Using the above equation and the beam formula

$$M_o = \frac{bh^2}{6} \sigma \tag{17}$$

together with $F_x = \frac{W}{g} \ddot{\Delta}_x$

the expression for $\frac{\ddot{\Delta}_x}{g}$ is obtained as

$$\frac{\ddot{\Delta}_x}{g} = \frac{6 (1 + c) + \beta_1}{3 (1 + 2c) + \beta_1} \frac{\sigma b h^2}{3 \ell_f W} \tag{18}$$

For satisfying the condition of equal rigidities, the last equation takes the new form

$$\frac{\dot{\Delta}_x}{g} = \frac{6(1 + c) + \beta_1}{3(1 + 2c) + \beta_1} \frac{\sigma}{3 \ell_f W} \gamma b^3 \tag{19}$$

D. Fork Dimension Versus the Applied Force Normal to the Shaft

The moment M_o shown in Fig.21b is statically determinate. Hence,

$$M_o = \frac{F_y}{2} \ell_f \tag{20}$$

The beam formula is

$$\sigma = M_o / (hb^2/6) \tag{21}$$

Solving Eqs. (20) and (21)

$$F_y = \frac{\sigma b^2 h}{3 \ell_f} \tag{22}$$

If the condition of equal rigidities expressed by Eq. (13) is satisfied, the last equation becomes

$$F_y = \frac{\sigma}{3 \ell_f} \gamma^{1/2} b^3 \tag{23}$$

Let

$$F_y = \frac{W}{g} \dot{\Delta}_y$$

Substituting the above equation into Eq. (23) leads to

$$\frac{\dot{\Delta}_y}{g} = \frac{\sigma}{3 \ell_f W} \gamma^{1/2} b^3 \tag{24}$$

E. Fork Dimension Versus Temperature Differential

It is first necessary to determine the internal forces M and P (Fig. 21c). As explained on page 16 in Ref. 5, they are found from the two following equations for deflection and rotation.

$$P\left(\frac{\delta}{p}\right)_f - M\left(\frac{\delta}{m}\right)_f = \frac{1}{2}\ell_s \alpha_s \Delta T$$

$$P\left(\frac{\theta}{p}\right)_f - M\left(\frac{\theta}{m}\right)_f - M\left(\frac{\theta}{m}\right)_c = M\left(\frac{\theta}{m}\right)_s \tag{25}$$

Thus solving,

$$M = \frac{\frac{1}{2}\ell_s \alpha_s \Delta T \left(\frac{\theta}{p}\right)_f}{\left(\frac{\delta}{p}\right)_f \left[\left(\frac{\theta}{m}\right)_f + \left(\frac{\theta}{m}\right)_c + \left(\frac{\theta}{m}\right)_s\right] - \left(\frac{\delta}{m}\right)_f^2} \tag{26}$$

$$P = \frac{\left(\frac{\theta}{m}\right)_f + \left(\frac{\theta}{m}\right)_c + \left(\frac{\theta}{m}\right)_s}{\left(\frac{\theta}{p}\right)_f} M \tag{27}$$

Let

$$\left(\frac{\theta}{p}\right)_f = \left(\frac{\delta}{m}\right)_f = \frac{\ell_f^2}{2E_f I_f}$$

$$\left(\frac{\delta}{p}\right)_f = \frac{\ell_f^3}{3E_f I_f}$$

$$\left(\frac{\theta}{m}\right)_f + \left(\frac{\theta}{m}\right)_c = (1 + c)\frac{\ell_f}{E_f I_f} \tag{28}$$

$$\left(\frac{\theta}{m}\right)_s = \frac{\ell_s}{2E_s I_s^*}$$

Here $I_s^* = 1.64\, I_1$

Substituting Eq. (28) into Eqs. (26) and (27) give, respectively,

$$M = \frac{E_f \ell_s \alpha_s \Delta T\, bh^3}{4\ell_f^2 (2\beta + 4c + 1)} \tag{29}$$

where $$\beta = \frac{E_f \ell_s I_f}{E_s \ell_f I_s^*} \tag{30}$$

and $$P = (\beta + 2c + 2)\frac{M}{\ell_f} \tag{31}$$

Next, write the expression for M_o shown in Fig. 21c

$$M_o = P\ell_f - M$$

After substitution,

$$M_o = (\beta + 2c + 1)\frac{E_f \ell_s \alpha_s \Delta T\, bh^3}{4\ell_f^2 (2\beta + 4c + 1)} \tag{32}$$

Finally, M_o is related to the fork dimension through the beam formula

$$M_o = \sigma\,(bh^2/6)$$

Thus, this equation and Eq. (32) determine the relation between ΔT and the fork dimension as follows

$$\Delta T = \left(\frac{4\ell_f^2}{3E_f \ell_s \alpha_s} \cdot \frac{\beta + 2c + 0.5}{\beta + 2c + 1}\sigma\right)\frac{1}{h} \tag{33}$$

For the fork to satisfy Eq. (13)(the condition of equal rigidities) the above relation becomes

$$\Delta T = \left(\frac{4\ell_f^2}{3E_f \ell_s \alpha_s} \cdot \frac{\beta + 2c + 0.5}{\beta + 2c + 1}\sigma\right)\left(\frac{1}{\gamma}\right)^{1/2}\frac{1}{b} \tag{34}$$

F. Results

Fig. 22 shows the results, i. e. curves of h vs b, temperature vs b and acceleration vs b.

The following data are used in obtaining these curves:

$$\ell_s = 1.57 \text{ in.}$$

$$\ell_f = 0.716 \text{ in.}$$

$$I_1 = 0.578 \times 10^{-4} \text{ in}^4$$

$$I_f = 1.886 \times 10^{-4} \text{ in}^4$$

$$I_s = I_1$$

$$I_s^* \simeq 1.64\, I_1 = 0.948 \times 10^{-4} \text{ in}^4$$

$$W = 0.646 \text{ lbs.}$$

$$E = \begin{cases} 42.0 \times 10^6 \text{ psi} & \text{(Beryllium)} \\ 32.0 \times 10^6 \text{ psi} & \text{(Elkonite)} \\ 29.0 \times 10^6 \text{ psi} & \text{(52100 Steel)} \\ 10.8 \times 10^6 \text{ psi} & \text{(Aluminum)} \\ 6.5 \times 10^6 \text{ psi} & \text{(Magnesium)} \end{cases}$$

$$\alpha_s = \begin{cases} 7.4 \times 10^{-6} \text{ in/in/°F} & \text{(Beryllium)} \\ 4.72 \times 10^{-6} \text{ in/in/°F} & \text{(Elkonite)} \\ 6.9 \times 10^{-6} \text{ in/in/°F} & \text{(52100 Steel)} \end{cases}$$

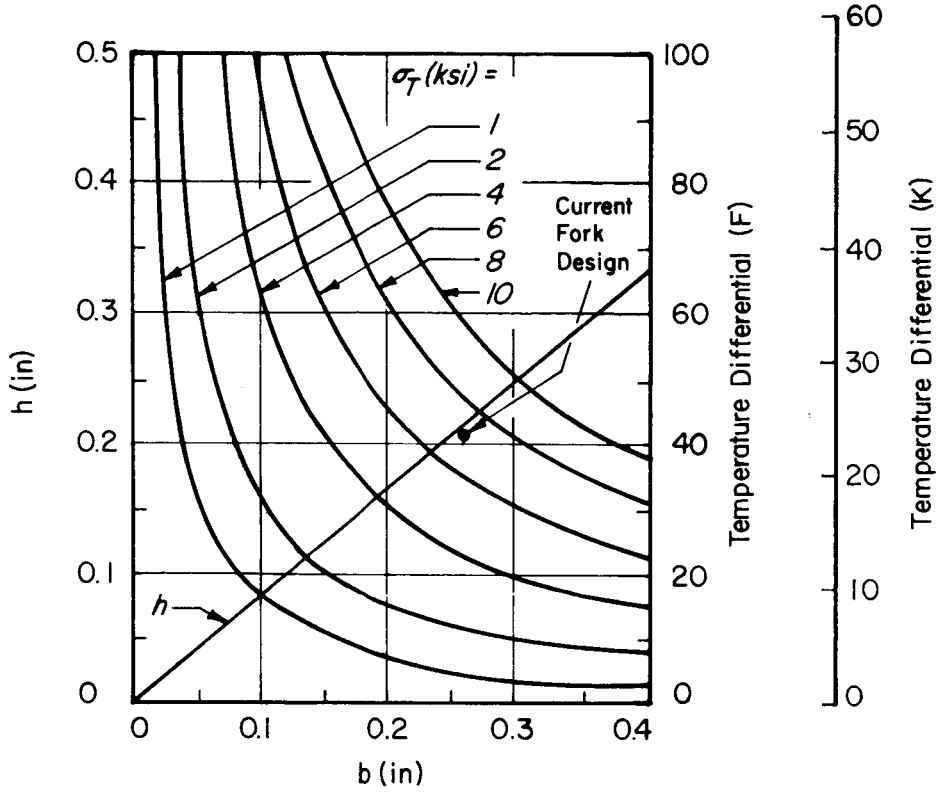

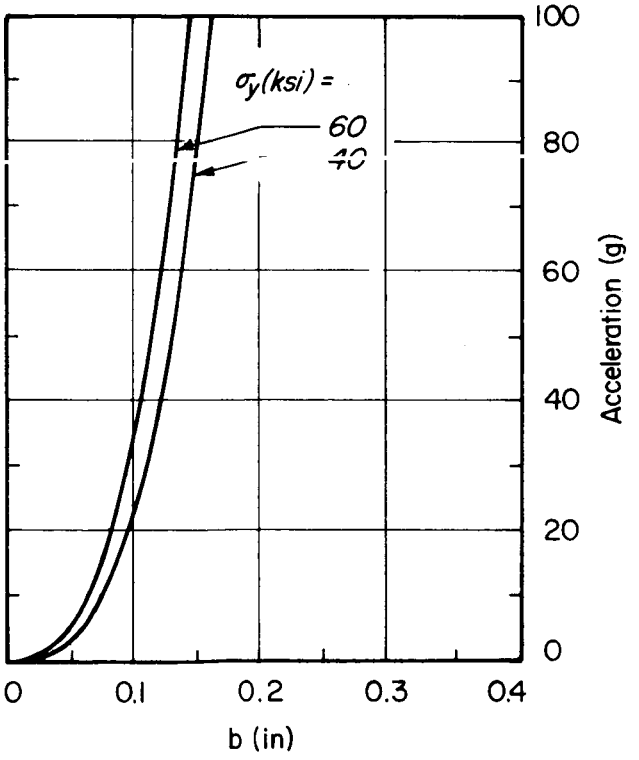

5817

5817a

(a) Beryllium Fork, Beryllium Shaft

Figure 22 Design Charts for Fork Dimensions for Temperature (top chart) and Acceleration (bottom chart)

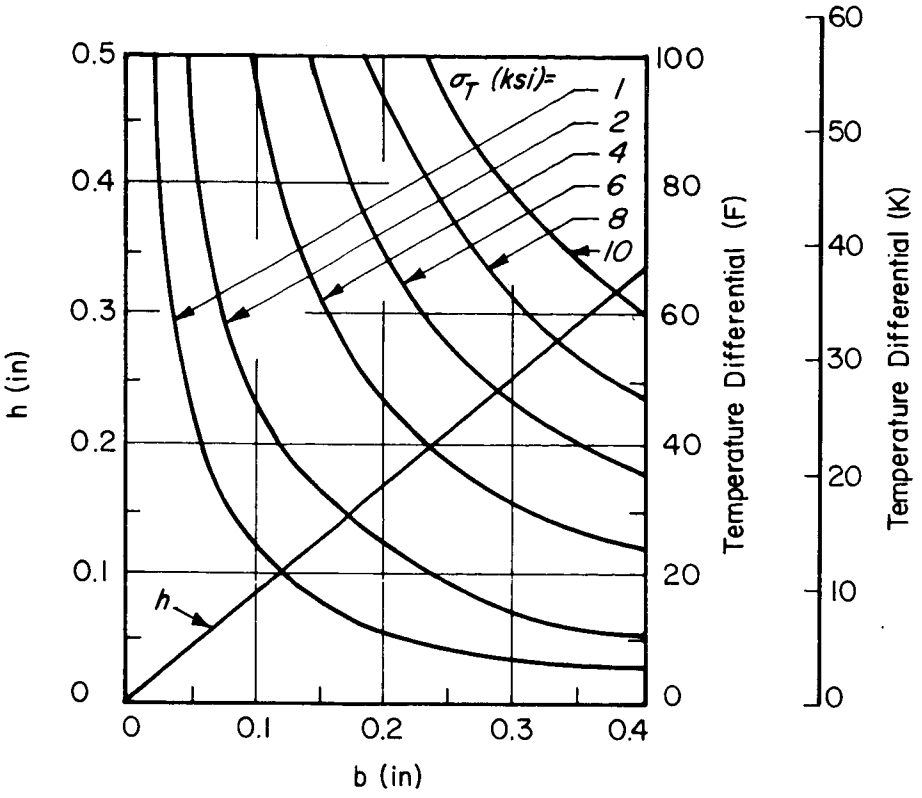

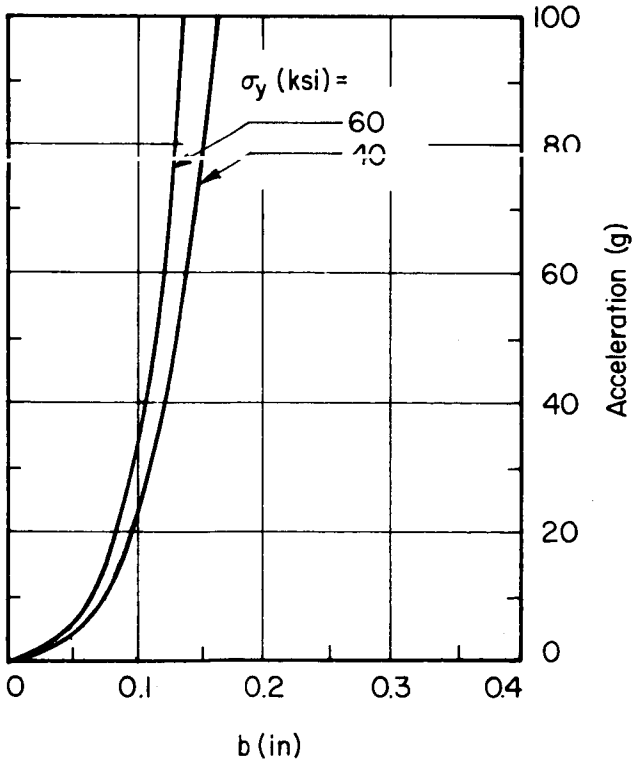

(b) Beryllium Fork, Elkonite Shaft

Figure 22 (continued)

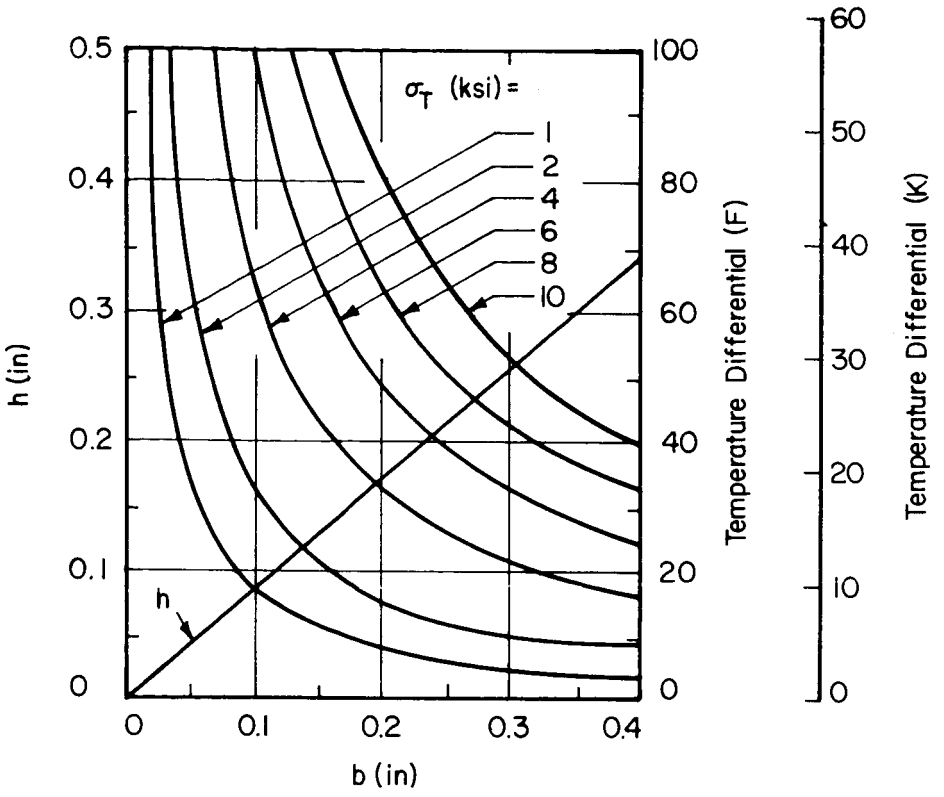

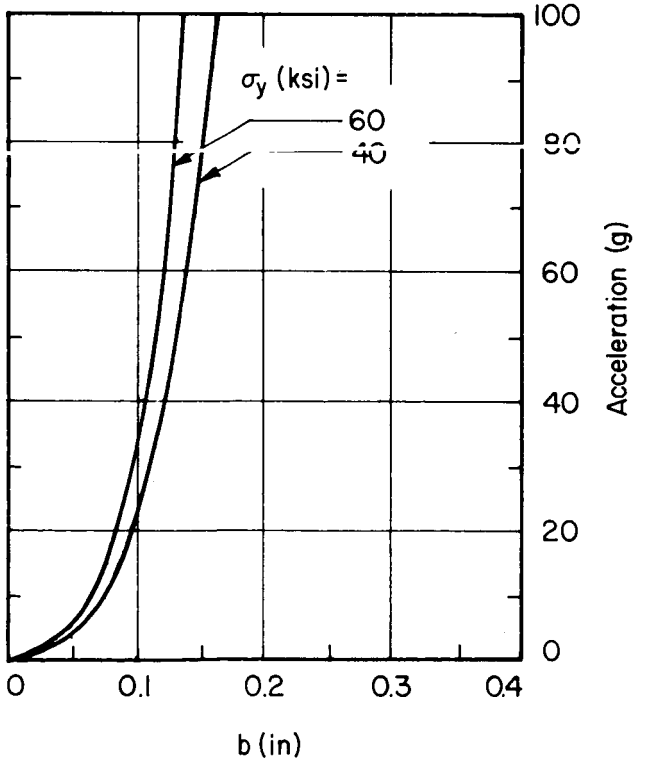

(c) Beryllium Fork, 52100 Steel Shaft

Figure 22 (continued)

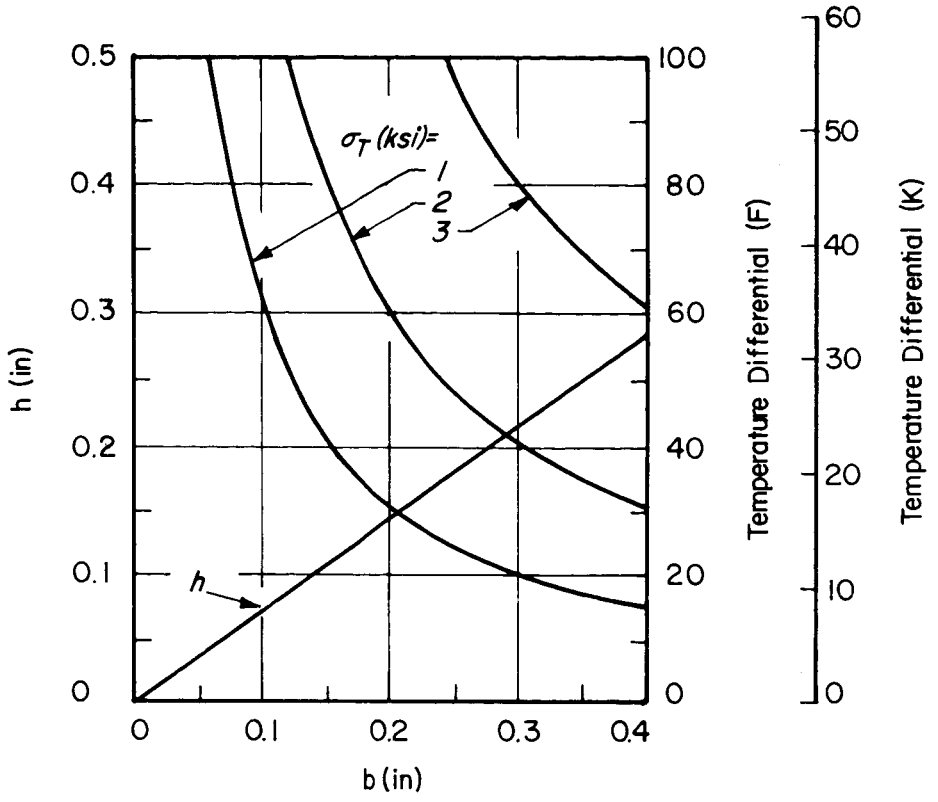

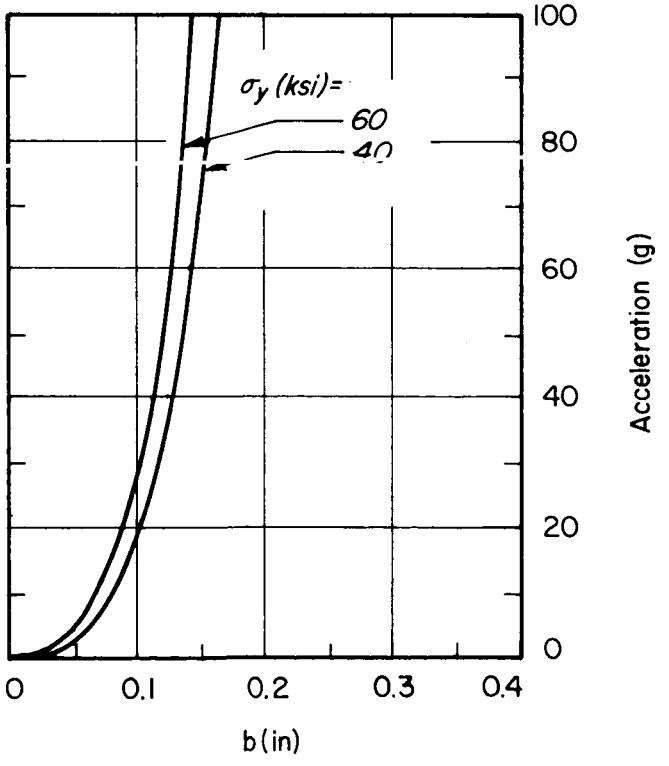

(d) Aluminum Fork, Beryllium Shaft

Figure 22 (continued)

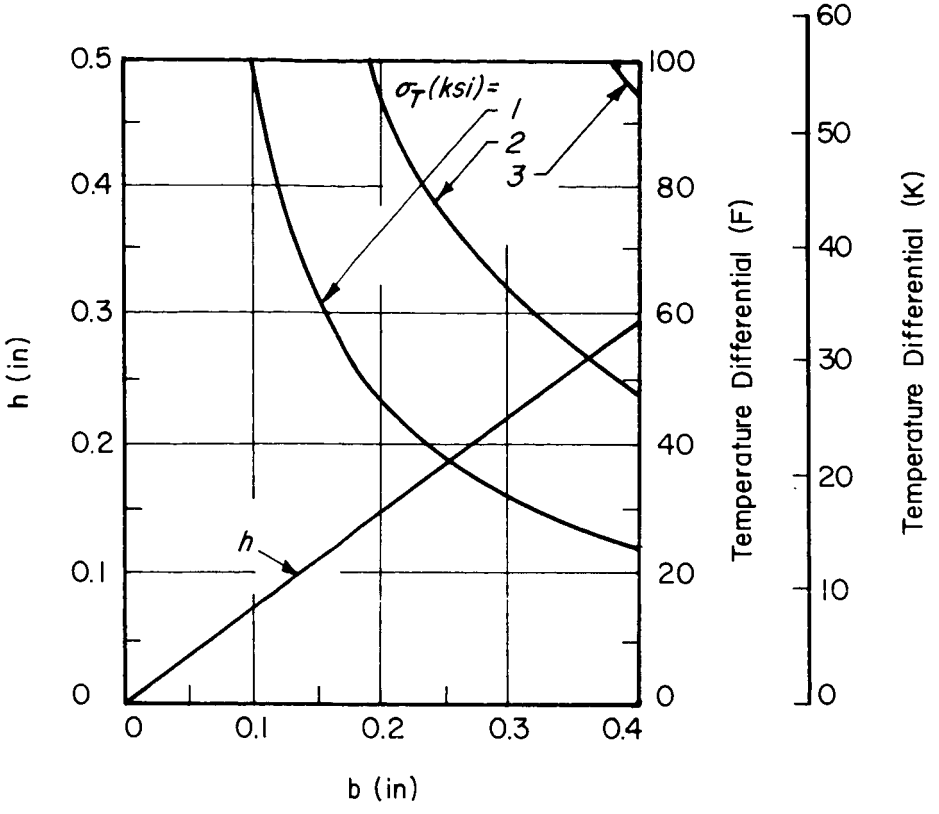

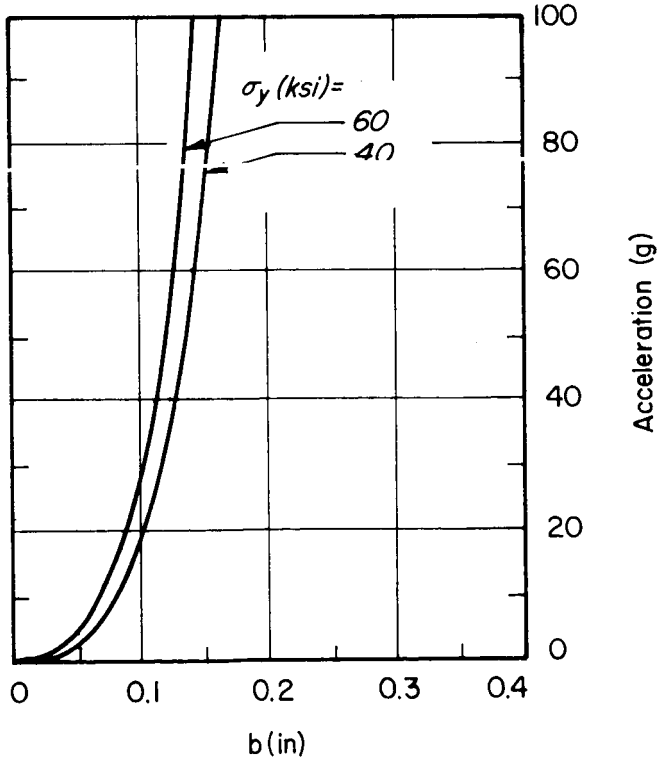

(e) Aluminum Fork, Elkonite Shaft

Figure 22 (continued)

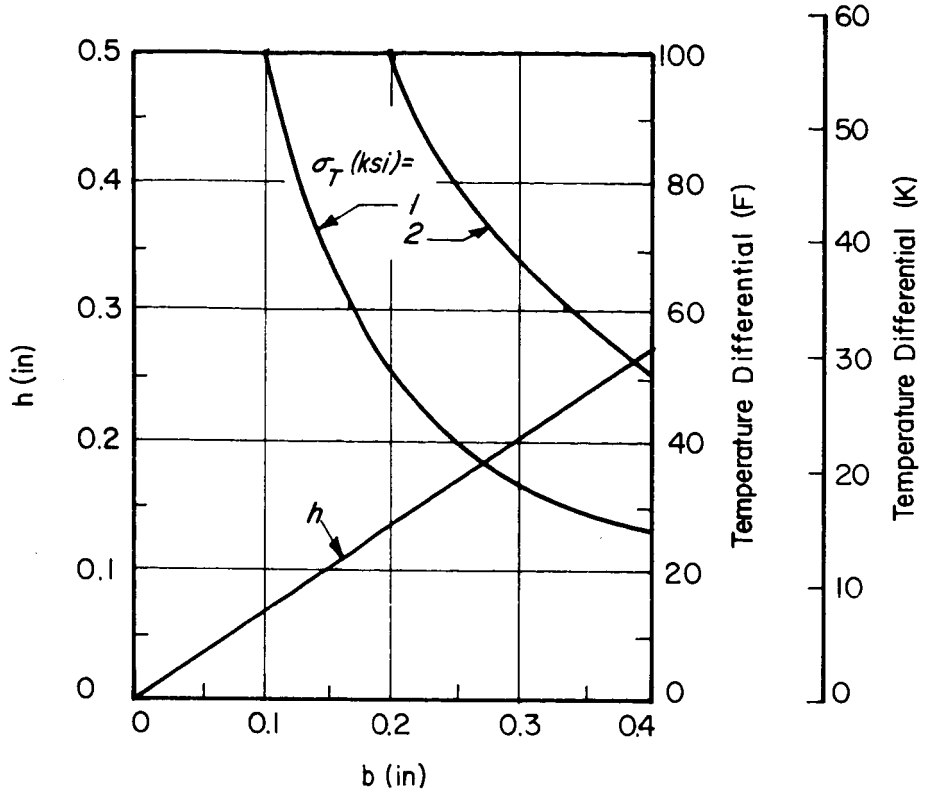

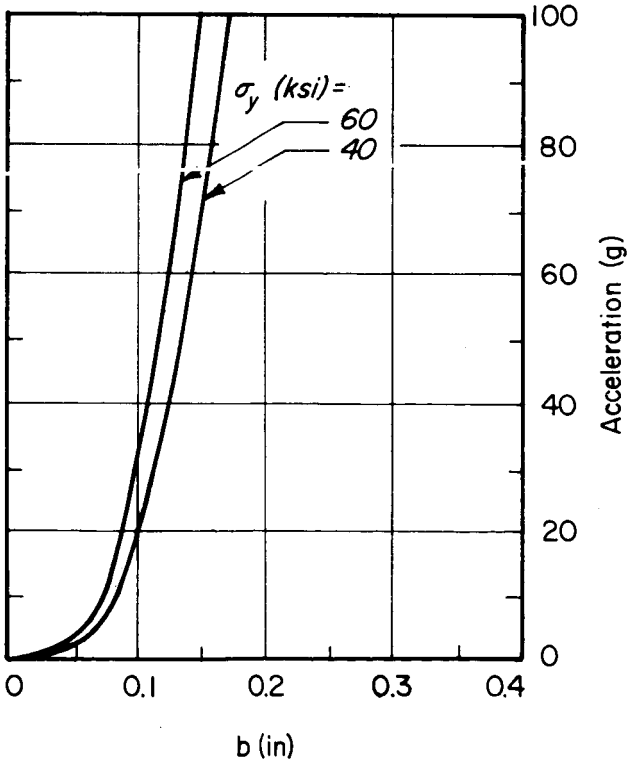

5869

5869a

(f) Magnesium Fork, Beryllium Shaft

Figure 22 (continued)

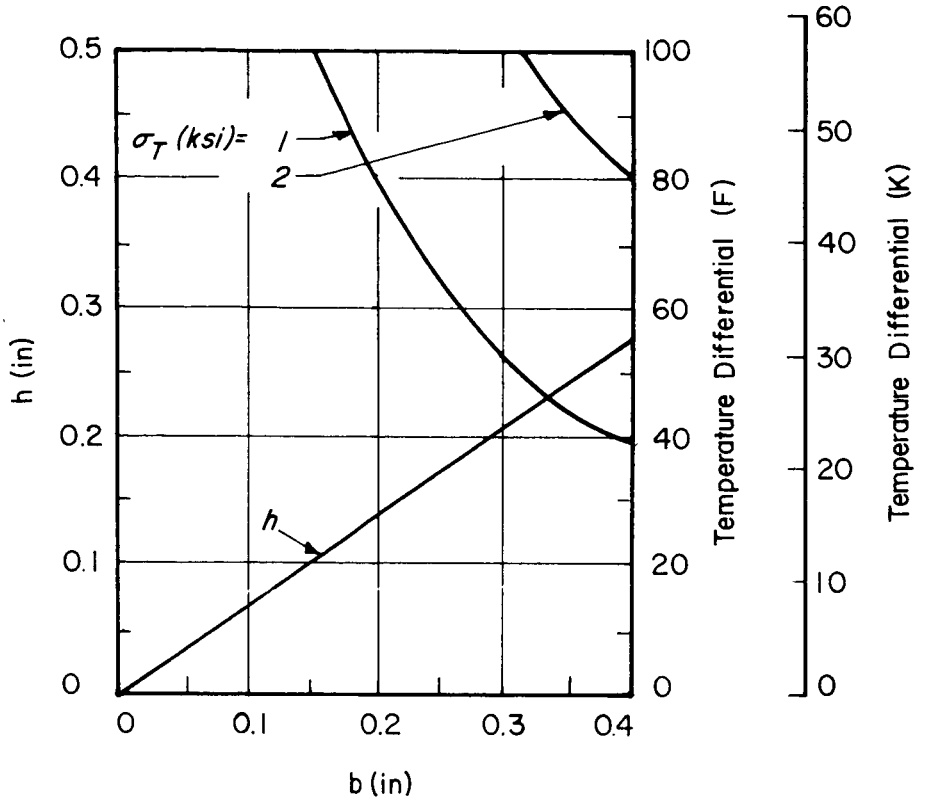

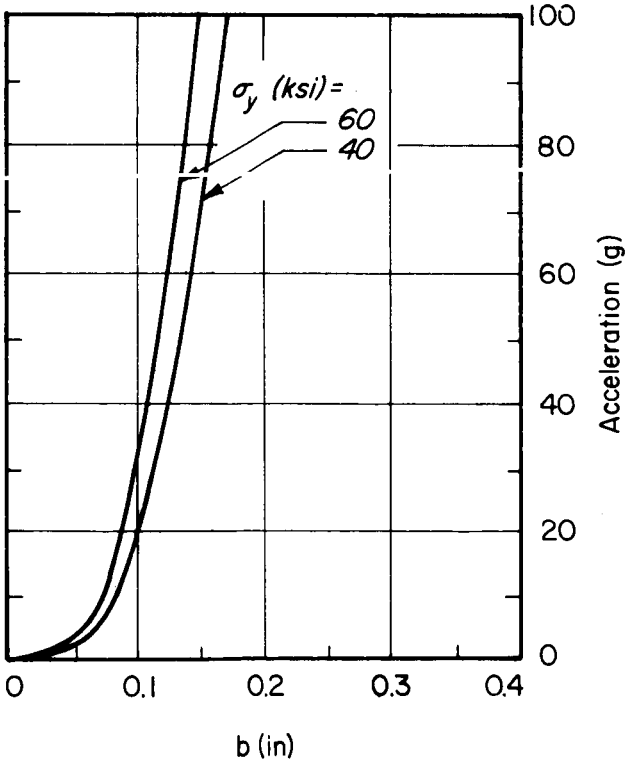

5870

5869a

(g) Magnesium Fork, Elkonite Shaft

Figure 22 (continued)

APPENDIX I

Treatments of Metals Tested

QMV Beryllium Rod - Bendix Spec. 450A Grade A (Brush S 100)

(1) Machined to within 0.010

(2) Vacuum stress relieved at 1325°F (990 K), 1 hr., furnace cooled.

(3) Finish machine

QMV Beryllium Rod -Bendix Spec. 450 A Grade D (Brush I 400)

Same as for Grade A above.

Berylco Lockalloy Rod

Used as received in annealed condition

52100 Steel Rod

(1) Rough Machine

(2) Heat treat - Austenitize at 1550 F (1120 K) 1/2 hour, Martemper in agitated salt 475 F (520 K) 3 to 5 minutes, Temper 300 F (420 K) (Hardness obtained Rockwell C 63.5-64)

(3) Grind

(4) Stabilize (a) 350 F (450 K) 1/2 hour hold (b) cool to R. T., (c) cool to 70 F (210 K) to 100 F (200 K) - 1/2 hour hold (d) warm to R. T., repeat a to d, reheat to 350 F (450 K) - 1/2 hour hold, cool to R. T.

(5) Finish grind

Elkonite Rod

Stress relieved after machining 600 F (589 K) 2 hours in inert atmosphere.

Appendix I

Chemical Compositions of Metals Tested

	Be	BeO	C	Fe	Al	Mg	Si	Mn	Each Other Metallic Impurity	Density lb/ cu in (gm/cc)
QMV Beryllium Rod Bendix Spec. 450 A Grade A (Brush S 100)	99.2	0.83	0.09	0.07	0.07	0.01	0.02	0.01	-.04	0.066 (1.84)
QMV Beryllium Rod Bendix Spec. 450 A Grade D (Brush I 400)	95.3	5.36	0.21	0.16	0.05	0.01	0.03	0.01	-.04	0.067 (1.88)
Berylco Lockalloy Rod	62.0	-	-	-	38.00	-	-	-	-	0.075 (2.08)

	Carbon	Mn	Si	Cr	P	S	Fe	Density lbs/ cu in (gm/cc)
52100 Steel Rod (Nominal Composition)	0.95-1.10	0.25-0.45	0.20-0.35	1.30-1.60	0.025 Max	0.025 Max	Bal	0.28 (7.8)

	Copper	Nickel	Silicon	Tungsten	Density lbs/ cu in (gm/cc)
Elkonite Rod Bendix Spec. 158	28.54	2.52	1.21	67.73	0.49 (13.8)

APPENDIX II

Temperature - Humidity Test Results

on Beryllium Samples

Conducted by Acton Laboratories, Inc.

According to

MIL-3-5272c, Procedure I

ACTON Laboratories, Inc.
533 MAIN STREET — ACTON, MASSACHUSETTS — COLONIAL 3-7756 BOSTON LIBERTY 2 0284
A SUBSIDIARY OF BOWMAR INSTRUMENT CORPORATION

ENVIRONMENTAL TEST DIVISION

REPORT OF TESTS

STARTING DATE: May 18, 1966
REPORT DATE : June 4, 1966

REPORT NO.	4581
MATERIAL	Three (3) ARA Beryllium Samples 1-S100, 1-I400, 1-BE38AL
YOUR ORDER NO.	Purchase Order No. 34636 Allied Research Associates
SUBMITTED FOR:	Moisture Resistance Test

1.0 REQUIREMENTS

Subject the above samples to Temperature-Humidity Test as required by MIL-E-5272C, Procedure I. Samples are to be visually examined daily.

2.0 PROCEDURES

The samples were suspended within a Blue M Humidity Chamber, Model FR386PC, and subjected to ten (10) 24-hour cycles of temperature-humidity as required by MIL-E-5272, Procedure I. Each sample was examined daily.

3.0 RESULTS

1st day	slight oxidation
2nd day	slight oxidation
3rd day	slight oxidation
4th day	slight oxidation
5th day	slight oxidation
6th day	slight pitting on all three (3) samples when viewed with microscope
7th day	slight pitting on all three (3) samples when viewed with microscope
8th day	slight pitting on all three (3) samples when viewed with microscope
9th day	slight pitting on all three (3) samples when viewed with microscope
10th day	slight pitting on all three (3) samples when viewed with microscope

4.0 DISPOSTION OF SAMPLES

The samples were returned to Allied Research Associates for further evaluation.

ACTON Laboratories, Inc.
531 MAIN STREET -- ACTON, MASSACHUSETTS — COLONIAL 3 7756 BOSTON LIBERTY 2 0284
A SUBSIDIARY OF BOWMAR INSTRUMENT CORPORATION

REPORT NO. 4581 REPORT DATE: June 4, 1966

Test conducted by,

Alfred C. Dentino

We certify that this report is a true report of the test conditions applied and the results obtained from our test of this material.

Respectfully submitted,

ACTON LABORATORIES, INCORPORATED
Subsidiary of
Bowmar Instrument Corporation

Marvin L. Tolf, Manager
Environmental Test Division

MLT:WJS/hmf

REFERENCES

1. Becker, H., Bird, F. F., Kyle, P. E., Papirno, R. P., Tang, C. N., "Photomechanical Investigation of Structural Behavior of Gyroscope Components, Task IV, Analysis of Initial Redesign of AB 5-K8 Gyroscope," Final Technical Report, ARA 284-8, prepared by Allied Research Associates, Inc., For NAS8-11294, Astrionics Laboratory, NASA, Huntsville, Alabama, April 1966.

2. Reichenbach, G. S., Brown, D. A. and Russell, P. G., "Yield Behavior of Certain Alloy Steels at Low Strain Values," Transactions Quarterly of American Society for Metals, Vol. 54, No. 3, Sept. 1961.

3. Jennings, C. G., et al, "Measurement of Inertial Guidance Material Dimensional Instability Parameters Using Resistance Strain Gages," presented at ASTM-ASM Symposium on Precision Mechanical Property Measurements, Atlantic City, New Jersey, 27 June 1966.

4. "The Metal Beryllium" p. 530-531, American Society for Metals, 1959.

5. Becker, H., Hultin, R., Kyle, P. E., "Photomechanical Investigation of Structural Behavior of Gyroscope Components, Task I," Allied Research Associates, Inc., Report No. ARA-F-284, July 9, 1965.